Marcos João do Carmo Gouveia

Simulating Vessel Growth with Extracellular Matrix Remodeling

Dissertation presented to the Physics Department at
University of Coimbra to obtain the Master's degree in Physics

July 2017

UNIVERSIDADE DE COIMBRA

Simulating Vessel Growth with Extracellular Matrix Remodeling

Marcos João do Carmo Gouveia

Supervisor:

Doutor Rui D.M Travasso

• U  C •

A thesis written in fulfillment of the requirements

for the Master's degree in Physics

Faculty of Science and Technology

Physics Department

Universidade de Coimbra, Portugal

Abstract

Sprouting angiogenesis is a mechanism the body uses to create new capillaries that will deliver oxygen and nutrients to the cells that constitute the surrounding tissue. This process is characterized by the protrusion of new sprouts from a preexisting vessel, a consequence of endothelial cell migration and proliferation. What makes angiogenesis so complex is that it involves chemical signaling, mechanical forces between the cells and the extracellular matrix, and endothelial cell coordination.

In this work we are interested in studying how the mechanical properties of the extracellular matrix influences endothelial cell's migratory behavior and how some cells are capable of changing those properties by degrading the collagen that forms the matrix. Using a continuous approach, we developed a phase field model from where we derive a set of partial differential equations that describe the dynamics of the vascular network as well as the reaction-diffusion processes that occur in parallel. One of the main advantages of this model is that it has a reduced number of parameters, whose value can be estimated based on experimental results. To solve the model we developed software capable of integrating the equations numerically and simulating the rule–based dynamics of endothelial cell activation.

The results we obtained allow us to characterize how endothelial cell migration is influenced by the mechanical properties of the matrix, especially its rigidity. For substrates with low rigidity the cells tend to separate from the starting vessel and migrate alone. On the other hand, stiffer matrices allow for the elongation of sprouts to occur, resulting in new, well structured vessels. We also characterize the role matrix metalloproteinases have in successful endothelial cell migration.

Resumo

A angiogénese é o mecanismo que o corpo utiliza para criar novos capilares que levarão oxigénio e nutrientes às células do tecido vizinho. Este processo é caracterizado pela protrusão de novos vasos a partir de um pré-existente, acompanhado por migração e proliferação das células endoteliais. O que torna a angiogénese tão complexa é o envolvimento de sinais químicos, forças mecânicas entre as células e a matriz extracelular, e coordenação entre as células endoteliais.

Neste trabalho, estamos interessados em estudar em que medida as propriedades mecânicas da matrix extracelular influenciam o comportamento migratório das células e como algumas delas são capazes de alterar essas propriedades, degradando o colagénio que forma a matriz. Usando um modelo contínuo de campo de fases, derivamos um conjunto de equações diferenciais com derivadas parciais que descrevem a dinâmica da rede vascular, assim como os processos de reação-difusão que ocorrem em paralelo. Uma das principais vantagens do modelo é o seu reduzido número de parâmetros, cujo valor podemos estimar baseando-nos em resultados experimentais. Para resolver o modelo, desenvolvemos um programa capaz de integrar as equações numericamente, ao mesmo tempo que impõe um conjunto de regras ao comportamento das células endoteliais.

Os resultados obtidos permitem-nos concluir que a migração de células endoteliais é influênciado pelas propriedades mecânicas da matriz, principalmente pela sua rigidez. Para substratos com baixa rigidez as células tendem a separar-se do vasos principal e migrar sozinhas. Por outro lado, matrizes muito duras facilitam a elongação dos vasos, dando a origem a novos vasos bem estruturados. Vimos também que a ação das metaloproteínases é essencial para a migração das células endoteliais.

Contents

List of Figures

List of Tables

Glossary

- **Anastomosis**: When to vessels connect to form a circuit for blood to flow.
- **Angioblasts**: Endothelial cell precursors.
- **Angiogenesis**: Formation of new blood vessels from preexisting ones.
- **Basement Membrane**: Thin layer that separates the endothelial tissue from the extracellular matrix.
- **Endothelial Cell**: Cells that compose the endothelium, which is the main constituent of capillaries.
- **Extracellular Matrix**: Collection of fibers and proteins that provides support to the surrounding cells and structures.
- **Hypoxia Inducible Factor**: Formation of new blood vessels from precursor cells.
- **Knockout Mice**: Formation of new blood vessels from precursor cells.
- **Matrix Metalloproteinases**: Formation of new blood vessels from precursor cells.
- **Notch Mechanism**: Formation of new blood vessels from precursor cells.
- **Phalanx Cell**: Formation of new blood vessels from precursor cells.
- **Stalk Cell**: Formation of new blood vessels from precursor cells.
- **Tip Cell**: Formation of new blood vessels from precursor cells.
- **Vasculogenesis**: Formation of new blood vessels from precursor cells.

List of Abbreviations

CH	Cahn–Hilliard
CPM	Cellular Potts Model
EC	Endothelial Cell
ECM	Extracellular Matrix
FFT	Fast Fourier Transform
FGF	Fibroblast Growth Factor
FTCS	Forward Time Centred Space
HIF	Hypoxia Induced Factor
KGF	Keratinocyte Growth Factor
MMP	Matrix Metalloproteinases
PDE	Partial Differential Equation
TC	Tip Cell
TIMP	Tissue Inhibitor of Metalloproteinase
TGF	Transforming Growth Factor
VEGF	Vascular Endothelial Growth Factor

Chapter 1

Biological introduction

Before developing a mathematical model to describe a certain physical system, be it a cell or a black hole, it is essential to know as much as we can about it in order to identify and understand the key mechanisms that lead to the properties we are interested in studying. When building a model around a biological system, like in our case, we have to grasp the essential processes that occur and the entities that play a part in it. These include types of cells and tissues, chemical signals and other pathways that coordinate in order for the system to work the way it does.

In this first chapter, we introduce important concepts related to angiogenesis using an hands-on approach for non–biology specialists and without going into too much detail.

1.1 Angiogenesis – Overview

The animal body is a highly complex and dynamic system which undergoes continuous change and renovation. This property becomes stunning when we think, for instance, in the time it takes for the cells in the lining of our stomach's to be renewed. If you are reading this, let us say, on a Monday, by Friday the cells of your stomach's inner surface will not be the same as when you started (due to the low pH environment they do not last very long).[1] Almost all tissues that constitute our organs undergo this process,

[1] On a philosophical note: We may be nothing more than a flesh and bone ship of Theseus.

although the time it takes for this cycle to complete varies from days to years.

One vital part of our body that is also in constant reconstruction is our circulatory system, for both physiological and pathological reasons. Due to the short length of diffusion of oxygen in the tissues, blood vessels are destroyed and created to guarantee that sufficient irrigation reaches the cells that are in hypoxia or in need of nutrients and other essential substances, establishing extremely complex networks (Figure 1.1). Cells also use these networks to get rid of byproducts that result from their metabolism, like carbon dioxide ([1]), and that are poisonous to themselves. Since every organ in our body is made up of cells, the circulatory system covers its entirety, from our brain to our toes.

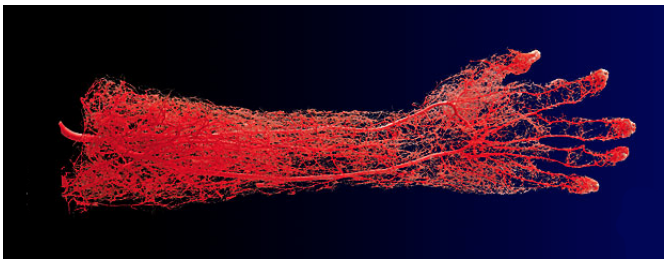

Figure 1.1: Blood vessel network in the human arm.

It is important to distinguish the two processes that give rise to the formation of new blood vessels, for they are sometimes taken to be the same thing.

- Vasculogenesis: *De novo* formation of blood vessels, which involves the differentiation of new endothelial cells from their precursors (called angioblasts) recruited directly from the bone marrow.

- Angiogenesis: New blood vessels are arise from preexisting ones.

In the context of this work, we will focus only on the second one, specifically on sprouting angiogenesis, a process where tubular structures (referred to as sprouts) made up of endothelial cells start diverging from an initial vessel forming new ramifications. The other way new capillary are formed from preexisting vessels is called intussusceptive angiogenesis or simply, splitting angiogenesis. There, a functional blood vessel splits

in two, originating new ramifications separated by a newly formed arterial wall. An illustration of the two kinds of formation are show in Figure 1.2.

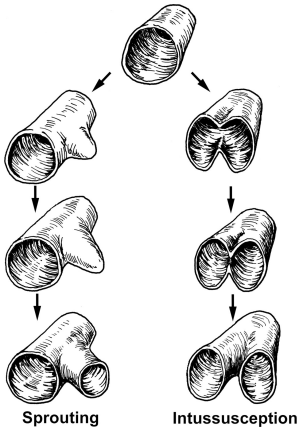

Figure 1.2: Diagram showing the two possible angiogenic processes [2].

The excessive and lack of occurrence of sprouting angiogenesis have been linked to the development of many disorders such as blindness (in diabetic patients) ([3]) and rheumatoid arthritis ([4],[5]), in the first case and heart disease ([6],[7]), ulcers ([8]) or wound healing problems ([9]) in the second. Also angiogenic activity is one of the main mechanisms involved in solid tumor growth ([10]), since their appearance is accompanied by the recruitment of new blood vessels to feed itself and to help its spreading and metastasis. For these reasons angiogenesis is considered one of the hallmarks of cancer ([11]).

Therefore it is of utmost importance to gain a proper understanding of the mechanisms behind sprouting angiogenesis as well as the conditions of the cellular environment that inhibit or enhance its occurrence. What makes it such a complex (and interesting) phenomenon is that it is only possible because of the perfect synchronization between many different processes and parts. Involved in angiogenesis are chemical (growth factors, proteins, oxygen, ...) and mechanical factors, as well as collective endothelial cell coordination ([12]). The contribution of these phenomena to angiogenesis is still not completely clear, namely the mechanical sub-processes, which makes it an active area of research and collaborative work between the exact science community (physicists,

mathematicians, computer scientists) and the medical experts, each delving into its theoretical and experimental aspects, respectively.

The process of sprouting angiogenesis can be divided into three major steps, illustrated in Figure 1.3 :

1. Tissue cells in an hypoxic state produce and release VEGF–A to the extracellular matrix (a).

2. VEGF and other pro-angiogenic diffusible proteins reach the blood vessels which respond by producing sprouts that migrate in the direction of the starving cells (b).

3. Those sprouts fuse together (anastomosis) to form a functional network where blood can now flow, supplying oxygen to the cells. Meanwhile, production of pro-angiogenic proteins ceases and angiogenic activity decreases (c).

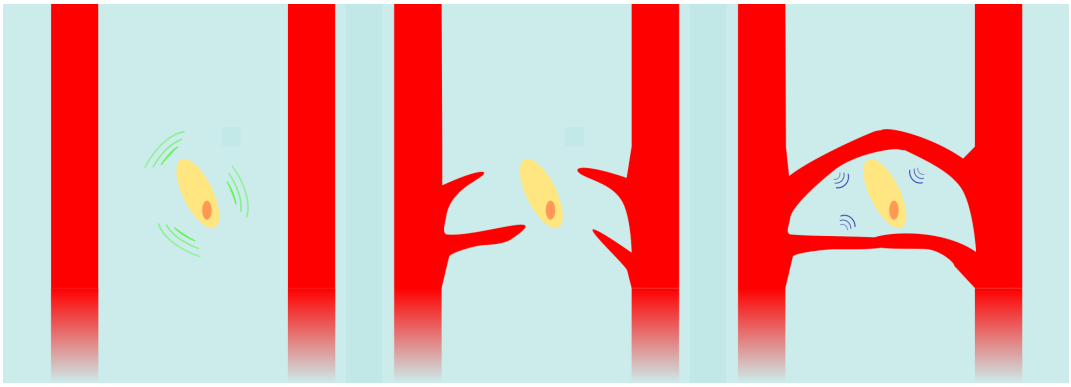

(a) (b) (c)

Figure 1.3: Three main steps in sprouting angiogenesis.

A more detailed explanation of the complex mechanisms behind these steps will be provided in the following sections.

1.2 Endothelial cells

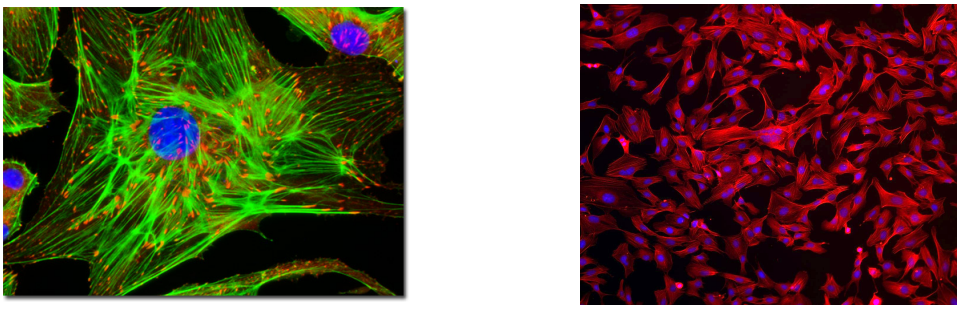

(a) (b)

Figure 1.4: Individual (a) and coordinated (b) endothelial cells [13].

Endothelial cells compose a single cell–thin layer lining the inside of blood and lymphatic vessels (called the endothelium) all around the circulatory system, from the thinnest capillaries to the largest arteries, such as the aorta. In larger vessels, the endothelium makes up only a small portion of the vessel's structure, sitting on top of muscle and elastic fibers. However, in capillaries they sit on top of the basement membrane and are responsible for the integrity of the entire vessel's wall.

The main function of the endothelium is to control the passage of material from the vessels to the surrounding tissue and vice versa. For this reason the endothelium is considered selectively semi-permeable. White blood cells, for instance, must leave the blood vessels to fight infections in various tissues. In the brain, this function is essential, since it stops bacteria and unwanted material to cross to the neurons, while allowing essential nutrients to pass.

Endothelial cells are also responsible for the dilation and contraction of blood vessels, which is a requirement for the organism to adapt to certain conditions.

The reason why these cells are important in the context of this thesis is because they are responsible for the structure of new blood vessels, meaning they are the main cell type involved in angiogenesis.

Endothelial cells can express different phenotypes, conferring them distinct charac-

teristics. This property will be made clear in further sections for it is one of the key mechanisms in sprouting angiogenesis.

1.3 VEGF signaling

VEGF stands for vascular endothelial growth factor and there are 7 different proteins that belong to the VEGF family and intervene in different physiological/pathological processes related to the formation of new vessel like structures. The occurrence of angiogenesis and vasculogenesis is highly dependent on the existence of growth factors, which are signaling proteins found in the ECM that promote the proliferation of endothelial cells. There are many families of growth factors, such as FGFs, KGFs, TGFs and VEGFs, the last ones being the most important in the context of angiogenesis.

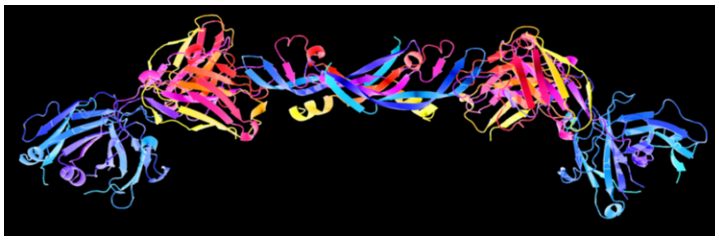

Figure 1.5: 3D representation of the VEGF molecule [14].

Table 1.1: Different kinds of VEGF and the processes where they are involved.

Protein	**Function**
VEGF-A	Angiogenesis
VEGF-B	Embryonic angiogenesis.
VEGF-C	Lymphangiogenesis
VEGF-D	Lymphangiogenesis in the lungs
PLGF	Vasculogenesis and wound healing

Since we are focusing on the study of angiogenesis the properties and the role of VEGF–A are the most interesting for us. VEGF–A can present itself in 8 isoforms:

VEGF–A_{121}, VEGF–A_{145}, VEGF–A_{148}, VEGF–A_{165}, VEGF–A_{183}, VEGF–A_{189}, VEGF–A_{206} and VEGF–A_{110}. The existence of these isoforms is a result of the alternative splicing process of exons present in the gene that encodes the production of VEGF–A and different kinds of VEGF–A have different affinities to cell membrane receptors. From this point on we will refer to VEGF–A simply as VEGF.

One interesting property of VEGF is that it can exist in both soluble and insoluble forms. The soluble VEGF is freely diffusible on the ECM, possessing very high motility. On the other hand, there are insoluble forms of the growth factor that are bound to the matrix ([15]) and are released more slowly, partly due to the action of the MMPs that degrade the collagen trapping the VEGF molecules in the ECM.

Some phenomena that are crucial to the process of angiogenesis and depend on the concentration/gradient of VEGF–A are endothelial cell migration ([16]) and proliferation, lumen development and the secretion of metalloproteases ECM by ECs. The importance of VEGF in angiogenesis is backed by experiments performed in knockout mice, where they observed that the loss of a single VEGF–A allele results in embryo fatality due to abnormal or absent capillary formation [17].

1.3.1 VEGF production

The production of VEGF by tissue cells in environments with low oxygen concentration is the trigger for the formation of new blood vessels. Inside the cell exists a transcription factor for VEGF called HIF–1 (hypoxia inducible factor), a dimer made up of HIF–1α and HIF–1β.

In the presence of oxygen, both of these factors are produced at a certain rate but HIF-1α is immediately decomposed in the cell into its constituents, meaning there will be no dimer formation and the production of VEGF will not happen. However, in hypoxia, the two monomers meet in the nucleus forming HIF–1 which serves as a transcription factor, leading to the production of the growth factor.

The VEGF is then released to the ECM and starts diffusing, creating a concentration gradient that will act as a breadcrumb trail for the sprouts to follow.

1.3.2 VEGF receptors

When VEGF molecules reach the vicinity of endothelial cells they attach to receptors located in the surface of the membrane ([18]). There are two main VEGF receptors:

- VEGFR1.
- VEGFR2.

Depending on what receptor captures the VEGF, different pathways are activated, which has different consequences in terms of the changes the endothelial cell will suffer. In sprouting angiogenesis the most important receptor is the VEGFR2 which is responsible for the pathway leading to the migratory behavior of tip cells (the concept of tip and stalk cell will be explained in the following sections). In turn, the VEGFR1 receptor is related to the proliferation and cell division of stalk cells, important for the structural integrity of the newly formed sprout.

1.4 Endothelial cell activation

The capability of endothelial cells to take on different roles during the angiogenic process is one of the key starting points for most theoretical models that try to explain the formation of new blood vessels. On the context of sprout formation, endothelial cells can be divided into two classes:

- Stalk cells
- Tip cells

A third class of cells called phalanx cells is sometimes considered too. These are endothelial cells that are not activated and remain quiescent, performing only a supporting role.

The process by which endothelial cells take on different roles occurs at a deeper level through the expression of certain genes. This difference is reflected on the way cells react

to the concentration of certain chemicals, their shape, and also on the presence of extra appendices/structures like filopodia.

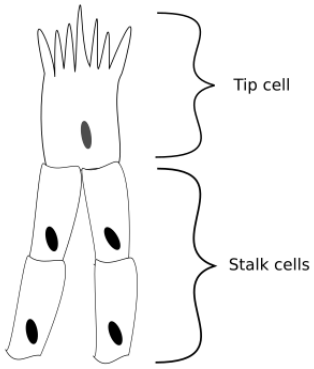

Figure 1.6: Illustrative diagram of a sprout.

1.4.1 Tip cells

The leading cells that guide the growth of the new sprout are called tip cells for they are located at the tip of the protrusion. The migratory behavior exhibited by tip cells can be explained by their higher motility when compared to regular endothelial cells which in turn is related to their different morphology and their response to the presence of growth factors. EC's that acquire this phenotype develop antenna-like structures called filipodia that scan the ECM for VEGF while also exerting traction forces, pulling along the rest of the sprout.

These specialized EC's are able to produce MMPs which degrade the basal membrane of the original vessel allowing for the forming sprout break through and invade the extracellular matrix starting the process of forming a new capillary. These matrixins also degrade surrounding collagen fibers allowing more room for the tip cell to advance, moving the vessel towards the hypoxic regions.

When different tip cells meet in space, they use their filipodia to connect and establish a new, functioning vessel network, allowing for blood to flow and irrigate the starving cells.

1.4.2 Stalk cells

While the function of the tip cell is to guide the new vessel sprout, other endothelial cells are in charge of maintaining its structural integrity. These cells proliferate, i.e. they divide by mitosis giving rise to new ones, thus strengthening the sprout. The recruitment of pericytes (supporting cells) and the formation of new basement membrane gives an extra sturdiness to the new capillary.

1.5 Tip cell selection

Now that we know that endothelial cells must undergo specification in order for sprouting angiogenesis to occur, we are interested in knowing how the role of each EC is decided. Why do some cells exhibit a migratory behavior, while others simply follow along?

The expression of the tip cell phenotype is related to their ability to detect the presence of growth factors such as VEGF and then follow its gradient towards the starving, hypoxic cell. Contrarily, stalk cells possess high proliferative potential, regulated by the presence of growth factors but have low migratory tendencies. Since the interaction between endothelial cells and VEGF happens through receptors located in the membrane of said cells, one way to solve the mistery of the different phenotype expression is by looking at the number of receptors each type of cell has in their surface. It was indeed observed that cells in a supportive role present less VEGF receptors than the cells that migrate, so there must be some kind of mechanism in action that suppresses the development of more binding sites for growth factors.

Studies on the formation of new arteries in the zebrafish revealed that something called Notch mechanism is responsible for this tip cell selection process. Specimens where this mechanism was suppressed showed an excessive amount of sprouting activity and its origin was tracked to the front of the new vessel. It was also shown that fish where the Notch activity was deficient presented a similar phenotype to embryos with deactivated VEGF pathways ([19]).

1.5.1 Notch signaling

In the context of angiogenesis, the Notch mechanism is thought to occur in two separate stages. First, the VEGF–A binds to the VEGFR2 receptors located in the surface of EC's leading to the production of delta-like ligand 4. Often referred as Dll4, it belongs to a family of proteins involved in this signaling pathway. Other members are Jag-1, Jag-2 and Delta-like-1,3.

Afterwards, Dll4 is captured by receptors in the neighboring cells and the expression of the gene responsible for the production of their VEGFR2 receptors is severely diminished. This numbs the sensing of VEGF by those cells reducing the probability of them becoming tip cells.

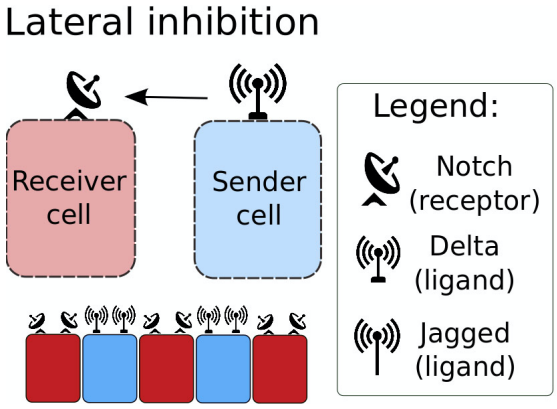

Figure 1.7: Lateral inhibition through Delta–Notch mechanism [20].

This process is called lateral inhibition, meaning the existence of a tip cell at a certain spot inhibits the activation of other ECs to the same phenotype in its neighborhood ([21]). Lateral inhibition occurs between cells that are directly in contact, for there is no diffusion of any chemical responsible for the signaling process that would allow a "wireless" communication.

1.6 Mechanical factors in angiogenesis

1.6.1 Tip cell traction force

The importance of chemical signaling in angiogenesis has long been recognized and studied over the years. However, these factors are not enough to explain how the cells move, making their way through the ECM.

It is known that tip cells exert traction forces on the ECM and surrounding tissues, that allows them to progress, while pulling along the stalk part of the sprout, maintaining the connection to the parent vessel ([22]).

These traction forces have been measured for endothelial cells during the process of changing their shape, while spreading on the ECM ([23]). In Figure 1.8 we see a diagram of that force, determined experimentally, when the endothelial cell was in its relaxed state.

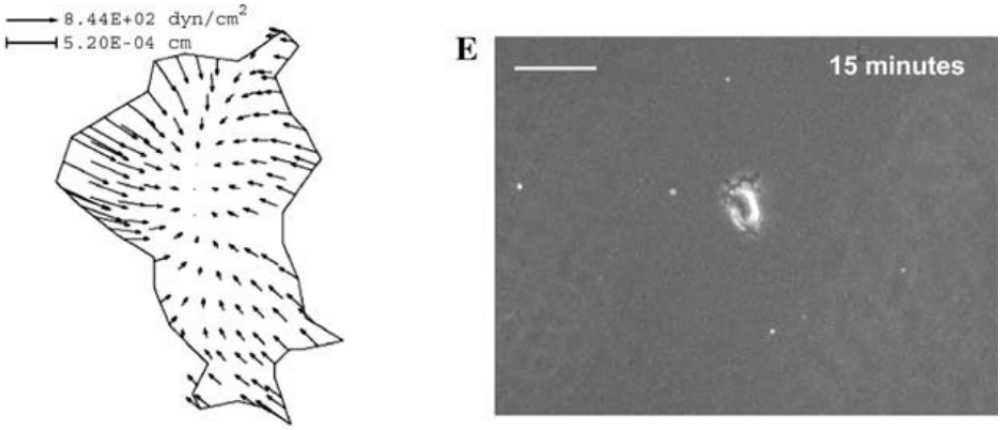

Figure 1.8: Diagram showing the traction force field inside an EC and the corresponding microscope image of said cell ([23]).

We can see the cell's force is directed towards its center and its intensity is maximum at the boundary.

Since the migration process of the endothelial cell and therefore the growth of the new sprout depends on the application of this traction force on the ECM, we are led to believe that the mechanical properties of the matrix may influence the way angiogenesis

occurs.

1.6.2 Mechanical properties of the ECM

The extracellular matrix is the medium that serves as substrate for the surrounding cells and in its constitution there are many fibers and proteins. It is composed mainly of collagen, responsible for its stiffness, and of elastin which provides the matrix with an elastic behavior allowing it to stretch when needed and after, to return to its relaxed state, just like a spring. Depending on the concentration of these two substances, the mechanical properties of the ECM can be very different from one tissue to the next. This difference can influence the way the cells behave and perform their functions.

Cell migration is also dependent on the stiffness of the matrix, and they are known to move along the gradient of rigidity. This guided cell movement is called durotaxis.

The ECM's integrity is not constant, for it is susceptible to remodeling processes and degradation due to the existence of matrix metalloproteinases.

1.7 MMP's and ECM remodeling

1.7.1 What are MMPs?

Matrix metalloproteinases, or as they are commonly known, MMPs, are a family of enzymes that play a fundamental role in angiogenesis. Their existence was first noted in 1962 by Gross and Lapiere while studying the metamorphosis process of the tadpole (larval state of some amphibian creatures). One of its stages consisted of the tail of the tadpole being dropped and the process of how this happened intrigued the pair of scientists. Eventually they discovered there was some kind of enzyme-like structure that destroyed the collagen that gives shape to the tadpole's tail. This enzyme was called collagenase which today is known as MMP-1.

Since then, over 20 types of MMP have been described, each having different efficiency when acting on different kinds of substrate and related to this we can further separate MMPs into families. Also, they can be found in places other than the ECM, for they

can be located in the membrane of some cells (transmembranal) just like VEGF can be found in soluble and bound state.

Table 1.2: MMP families

Class	**Members**
Collagenases	MMP-1,8,13
Gelatinases	MMP-2,9
Membrane-type	MMP-14,15,16
Matrilysin	MMP-7,26

MMPs are produced inside the nucleus of endothelial cells and are secreted, moving around the ECM by diffusion. At first they are not ready to start degrading fibers and need to be activated. They possess a structure that acts like a switch that needs to be destroyed in order for the MMP to do its job. Interestingly, this responsibility often falls on the shoulders of other MMPs, i.e. an activation chain is formed (Figure 1.9). The reason why this ON button is important is that MMPs are so good at degrading other proteins that they could eventually degrade themselves.

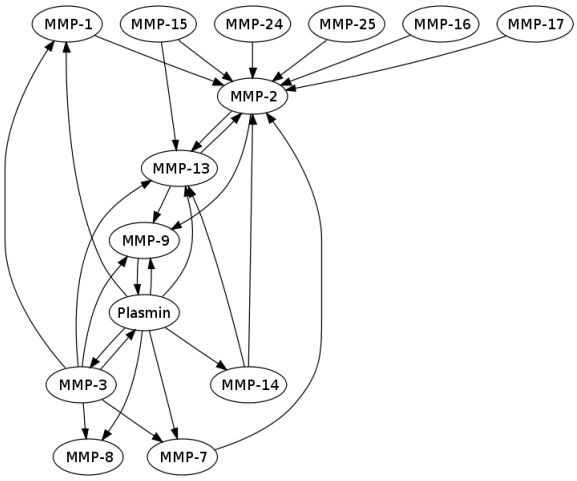

Figure 1.9: MMP activation chain [24].

A number of inhibitors are known to stop metalloproteanases from functioning cor-

rectly and they were given the name TIMPs, acronym for tissue inhibitor of metalloproteinases. The balance between the concentration of MMPs and its inhibitors is essential for the organism to function correctly, for example when it comes to wound healing. Experiments involving aortic tissue have revealed that the presence of MMPs is a must for the endothelial cells to move towards the wound site. In MMP transcription gene knockout mice endothelial cell migration was close to null, while in TIMPs knockout mice the damaged tissue was promptly healed.

Matrixins also play a part in the development of some cardiac diseases, seeing that it is involved, for instance, in the detachment of atherosclerotic plaque in blood vessels which can then lead to strokes and, eventually, death.

1.7.2 MMPs in angiogenesis

We have already established that tip cell migration through the ECM is probably the most important mechanism for angiogenesis. However, the extracellular environment is not homogeneous but instead is made up of fibers that become an obstacle, not allowing the leading cell to advance towards the hypoxic center. Thankfully, we know that they are able to overcome these barrier and that is mainly due to the activity of MMPs.

The role of the matrixins in this angiogenic play begins even before the tip cells starts its migration, because MMPs are responsible for the drilling of the basement membrane that surrounds the parent blood vessel, allowing the tip cell to break through and give rise to a new protrusion.

After that, something needs to be done regarding the hard fibers in the matrix. MMPs also take care of them, opening a trail for the sprout to progress.

1.8 Angiogenesis-related therapies

Since angiogenesis is one of the key processes involved in tumor growth and its spreading, it has been the target of some therapeutic procedures in cancer patients. In order to grow, tumor cells need nutrients and oxygen, just like regular, healthy cells, and

a new network must be established in order to provide them with those substances. This means that if we are able to cut off the blood supply to these malignant cells, they will eventually starve to death and the development of a potentially deadly cancer will be stopped.

This, however, was revealed to be a naïve approach to the problem for it was shown that disrupting the tumor's blood supply, only made it more agressive in the long run. An explanation for this fact is that when in an hypoxic environment, the migratory phenotype of the cancer cells became more active and the tumor would try to enter the nearby blood stream and spread to other organs and tissues.

Anti-angiogenic drugs can act by interfering with different processes, for they can attach to the VEGF molecule itself and inhibit its action or they can disrupt the VEGF receptors that exist in the membrane of ECs. Angiogenesis inhibitors have been used not only for cancer but for other diseases related to excess formation of vessels like macular degeneration and diabetic retinopathy.

Chapter 2

Relevant physical concepts

After we became acquainted with the biological background relevant to this thesis, we moved on to the mathematical and physical theory that is necessary to create an adequate model that describes the system's relevant processes as close to the biological reality as possible. The key concepts behind this work are related to the field of statistical mechanics, more specifically the theory of phase transitions, culminating in the phase field model which forms the starting point for the whole model. We also take a look at some of the basic theory of elastic interactions which is important to understand the mechanical interaction between cells and tissues involved in sprout formation. We start, however, by talking about the calculus of variations and the concept of a functional, essential in understanding the way we extract information from the system's free energy.

2.1 Calculus of variations

Most of the time when studying mathematics we deal with scalar functions, a concept we can compare to a "machine" that takes in a **number** and returns another **number**. For instance, if we define

$$f(x) = x^2$$

what f will do is take the provided value of x and return its square, both of them numbers.

We can now introduce the new concept we will call a functional which is another kind of "machine" that accepts **functions** as input and outputs a **number**. Perhaps the simplest example of a functional is the definite integral

$$F[f(x)] = \int_a^b f(x)\mathrm{d}x$$

and also

$$F[f(x)] = f(x_0)$$

where x_0 is some point that belongs to the domain of $f(x)$. Next, after studying functions and their properties we learned about the concept of limits and derivatives. If we wanted to know how the value of a function varies at a certain point we calculate its derivative there and examine the result. Returning to our $f(x)$, its derivative will be

$$\frac{\mathrm{d}f}{\mathrm{d}x} = 2x$$

Many times it is useful to know what happens to the value of a functional when the input function changes its shape. We define the functional derivative $\frac{\delta F}{\delta \phi}$ as

$$\delta F = F[\phi + \delta\phi] - F[\phi] = \int \frac{\delta F}{\delta \phi}\delta\phi \ \mathrm{d}x \tag{2.1}$$

There is a big difference of interpretation between the derivative of a function and a functional derivative, for in the first case we are measuring how the value of the function changes when the x value also changes. With functionals we are interested in how its value, which depends on the shape of the input function extending through the whole domain, changes when the shape is distorted.

Let us calculate the functional derivative of a functional $F[\rho]$ defined as

$$F[\rho] = \int_{-\infty}^{+\infty} \rho^{5/3}\mathrm{d}x \tag{2.2}$$

which appears in the context of the Thomas-Fermi model, where $\rho(x)$ is the electron density. We start by evaluating

$$F[\rho + \delta\rho] = \int_{-\infty}^{+\infty} (\rho + \delta\rho)^{5/3}\,\mathrm{d}x = \int_{-\infty}^{+\infty} \rho^{5/3}\left(1 + \frac{\delta\rho}{\rho}\right)^{5/3}\mathrm{d}x$$

and using the Taylor expansion

$$(1+x)^{5/3} \approx 1 + \frac{5}{3}x + \frac{5}{9}x^2 - \frac{5}{81}x^3 + \cdots$$

keeping the terms of $\delta\rho$ up to first order we get

$$F[\rho+\delta\rho] = \int_{-\infty}^{+\infty} \rho^{5/3}\mathrm{d}x + \int_{-\infty}^{+\infty} \frac{5}{3}\rho^{2/3}\delta\rho \ \mathrm{d}x = F[\rho] + \int_{-\infty}^{+\infty} \frac{5}{3}\rho^{2/3}\delta\rho \ \mathrm{d}x$$

From the definition of functional derivative in 2.1 we get

$$\frac{\delta F}{\delta \rho} = \frac{5}{3}\rho^{2/3}$$

Another example, this one well known to any physicist, are the Euler-Lagrange equations. One way to solve a mechanics problem, for instance, is to say that the trajectory a particle takes is the one that minimizes the action of the system. The action is defined as the integral of the Lagrangian

$$S = \int_a^b L(t, q_i, \dot{q}_i)\mathrm{d}t$$

We want to solve the equation

$$\begin{aligned}
\delta S &= \int_a^b L(t, q_i + \delta q_i, \dot{q}_i + \delta\dot{q}_i)\mathrm{d}t - \int_a^b L(t, q_i, \dot{q}_i)\mathrm{d}t \\
&= \int_a^b \frac{\partial L}{\partial q_i}\delta q_i \mathrm{d}t + \int_a^b \frac{\partial L}{\partial \dot{q}_i}\delta\dot{q}_i \mathrm{d}t \\
&= \int_a^b \left[\frac{\partial L}{\partial q_i} - \frac{\mathrm{d}}{\mathrm{d}t}\left(\frac{\partial L}{\partial \dot{q}_i}\right)\right]\delta q_i \mathrm{d}t + \frac{\partial L}{\partial q_i}\delta q_i\Big|_a^b \\
&= 0
\end{aligned} \tag{2.3}$$

If we assume that

$$\delta q_i(a) = \delta q_i(b) = 0$$

and since the minimization condition must be valid for any δq_i, we arrive at the famous Euler-Lagrange equations.

$$\frac{\mathrm{d}}{\mathrm{d}t}\left(\frac{\partial L}{\partial \dot{q}_i}\right) = \frac{\partial L}{\partial q_i} \tag{2.4}$$

These concepts of functional derivative will be important in the context of this dissertation for the system's free energy that will be presented in later sections, is a functional that we want to minimize.

2.2 Elasticity

Note: Based on [25] and [26].

When under the influence of an external force, a deformable body will change its shape and/or its volume. In a coordinate system, an infinitesimal portion of the body located at $\vec{r} = (x, y, z)$ is initially at rest and after the deformation that same mass element can be at a different position $\vec{r'} = (x', y', z')$. We define the displacement vector $\vec{u}$ as

$$\vec{u} = \vec{r'} - \vec{r}$$

and since the force that caused the deformation affects the body differently at distinct points, it is a function of the initial position, $\vec{r}$.

2.2.1 Strain tensor

Since the position of a point is altered after the deformation, the distance between two distinct points will also be different when the body changes shape.

Suppose we have two points A and B on a body at rest, initially separated by a distance l. After the deformation, the same points are now at their new positions A' and B', and the distance between them changed, and is now given by l'. The distance between two very close points is given by

$$\mathrm{d}l^2 = \mathrm{d}x^2 + \mathrm{d}y^2 + \mathrm{d}z^2$$

before the action of the external force and after the force is applied, this distance becomes

$$\mathrm{d}l'^2 = \mathrm{d}x'^2 + \mathrm{d}y'^2 + \mathrm{d}z'^2$$

If we write

$$\mathrm{d}x'_i = \mathrm{d}x_i + \mathrm{d}u_i = \mathrm{d}x_i + \frac{\partial u_i}{\partial x_j}\mathrm{d}x_j$$

(where $x \equiv x_1$, $y \equiv x_2$, $z \equiv x_3$ and the Einstein summation convention is implied) and assuming the deformation is very small, we can keep only first order terms, getting

$$\mathrm{d}l'^2 = \mathrm{d}l^2 + 2\varepsilon_{ij}\mathrm{d}x_i\mathrm{d}x_j$$

where we define the strain tensor components as

$$\varepsilon_{ij} = \frac{1}{2}\left(\frac{\partial u_i}{\partial x_j} + \frac{\partial u_j}{\partial x_i}\right)$$

We define the components such that the tensor is symmetric, meaning

$$\varepsilon_{ij} = \varepsilon_{ji}$$

We can interpret the ij component of the strain tensor as the variation of the displacement vector component i in the j direction. If we know the form of the strain tensor we know how the body's shape will be altered when a specific force is applied to it.

2.2.2 Stress tensor

A point that belongs to a body is in contact with its closest neighbors and they exert forces on each other on the surface that surrounds them. These can be split into shear stresses and pressures and if we assume that the force does not depend on the shape of surface, we can write

$$\mathrm{d}F_i = \sigma_{ij}\mathrm{d}S_j$$

where we can define σ_{ij} as the components of the stress tensor. The geometrical interpretation of its value is the tension in the i direction on a surface whose normal is in the j direction. For instance, the element σ_{xy} is defined as

$$\sigma_{xy} = \frac{x \text{ component of the force}}{\text{Area of a surface with its normal oriented in the } y \text{ direction}}$$

The diagonal elements of the tensor, σ_{ii}, represent normal tensions to the respective surface normals.

2.2.3 Equilibrium conditon

If we want to impose that the body is in an equilibrium state, we use the usual condition from classical mechanics

$$\sum_i \vec{F}_i = 0$$

The forces acting on each mass element of the body can be due to the interaction with its neighbors (surface) or they can be external forces like gravity (volumetric forces), for example. The equilibrium condition in this case is translated into

$$\oint_S \sigma_{ij} \mathrm{d}S_j + \int_V f_i \mathrm{d}V = 0$$

Using the Gauss theorem we can turn the integral over the closed surface as an integral over the enclosed volume of a divergence

$$\int_V \left[\partial_j \sigma_{ij} + f_i\right] \mathrm{d}V = 0$$

Since the above condition must be valid for any infinitesimal volume, we get

$$\partial_j \sigma_{ij} + f_i = 0$$

which is called Cauchy's equilibrium equation.

We can also show that the conservation of angular momentum forces the stress tensor to be symmetric, meaning

$$\sigma_{ij} = \sigma_{ji}$$

2.2.4 Elastic energy

Let us calculate the elastic energy associated with the deformations that occur in the body, by calculating the work done by the forces involved. Suppose that those forces cause an infinitesimal displacement δs_i on a certain point. Then, the work done by it can be written as

$$\begin{aligned}\delta U &= \oint_S \sigma_{ij} \delta s_i \mathrm{d}S_j + \int_V f_i \delta s_i \mathrm{d}V \\ &= \int_V \partial_j \left(\sigma_{ij} \delta s_i\right) \mathrm{d}V + \int_V f_i \delta s_i \mathrm{d}V\end{aligned}$$

Expanding the derivative of the product in the first term, we get

$$\delta U = \int_V \left[\left(\partial_j \sigma_{ij} + f_i\right) \delta s_i + \sigma_{ij} \partial_j \delta s_i\right] \mathrm{d}V$$

If the deformation is quasi-static, meaning after each displacement the system reaches a momentary state of equilibrium, the first term is zero, so

$$\delta U = \int_V \sigma_{ij} \partial_j \delta s_i \mathrm{d}V$$

Using the symmetry of the stress tensor and the definition of the components of the strain tensor, we can rewrite the above expression as

$$\delta U = \int_V \sigma_{ij} \delta \varepsilon_{ij} \mathrm{d}V$$

such that the energy density u can be defined as

$$\delta u = \sigma_{ij} \delta \varepsilon_{ij} \tag{2.5}$$

Using this expression we have a way of calculating the stress tensor components only by knowing the energy density and the strain tensor

$$\sigma_{ij} = \frac{\partial u}{\partial \varepsilon_{ij}} \tag{2.6}$$

2.2.5 Hooke's law

Since the stress tensor represents forces and the strain tensor represents the effect those forces have on a body, we are interested in writing an equation that relates the two tensors.

The most general way we can relate the causes and effects is by writing

$$\sigma_{ij} = \gamma_{ijkl} \varepsilon_{kl} \tag{2.7}$$

an equation known as the generalized Hooke's law, valid for linear deformations, where γ_{ijkl} is known as the elasticity tensor.

Using Hooke's law and equation 2.5, a small variation in the elastic energy density of the system can be written as

$$\delta u = \gamma_{ijkl} \varepsilon_{kl} \delta \varepsilon_{ij} = \frac{1}{2} \gamma_{ijkl} \delta (\varepsilon_{ij} \varepsilon_{kl})$$

and if we integrate both sides of the expression we get

$$u = \frac{1}{2}\gamma_{ijkl}\varepsilon_{ij}\varepsilon_{kl}$$

which has a similar form to the energy of the harmonic oscillator.

In the case where the material is isotropic and homogeneous, there are no preferential directions in the system so the elastic energy does not depend on those directions. Therefore, the energy must be invariant under any rotation operation. For these materials the components of the elasticity tensor have the form

$$\gamma_{ijkl} = \lambda\delta_{ij}\delta_{kl} + \tau\left(\delta_{ik}\delta_{jl} + \delta_{il}\delta_{jk}\right)$$

and so the energy density is given by

$$u = \frac{1}{2}\left[\lambda(\varepsilon_{ii})^2 + 2\mu\varepsilon_{ij}\varepsilon_{ij}\right] \tag{2.8}$$

where λ and μ are called the Lamé parameters.

Using 2.6 we can write the stress tensor components as a function of the strain tensor as

$$\sigma_{ij} = \lambda\varepsilon_{kk}\delta_{ij} + 2\mu\varepsilon_{ij}$$

which is called the Cauchy equation.

We can rewrite the equation using a couple of new parameters

$$\sigma_{ij} = K\delta_{ij}\varepsilon_{kk} + 2G\left(\varepsilon_{ij} - \frac{1}{d}\delta_{ij}\varepsilon_{kk}\right)$$

where K and G are the compressibility and rigidity constants, respectively. These are related to the Lamé parameters through

$$\lambda = K - \frac{2\mu}{d}$$
$$\mu = G$$

where d represents the dimensionality of the system [1].

[1] Throughout this thesis μ will be the symbol used for rigidity. We can do this since $G = \mu$

These two parameters can, in turn, be written in terms of the Poisson ratio (ν) and the Young's modulus (E), two characteristic properties of materials, as

$$\begin{aligned} \mu &= \frac{E}{2(1+\nu)} \\ K &= \frac{E}{3(1-2\nu)} \end{aligned} \tag{2.9}$$

Using these parameters is useful for they are observable quantities that can be easily measured for most of materials.

2.3 Landau theory of phase transition

Note: Based on [27] and [28].

Usually when looking for phase transitions on a certain thermodynamic system we start by analyzing it at the microscopic level, usually through the principles of statistical mechanics. In the end, we arrive at an expression for the free energy of the system, from where we extract relevant information about its behavior, such as entropy, specific heat, etc. We may also be interested in looking for discontinuities in some of these functions and if we find some, we can be in the presence of a phase transition. The problem with this approach is that a complete microscopic analysis of complex, many-particle systems is very hard, time consuming and, in most cases, impossible.

Landau's theory of phase transitions ([29]) is a phenomenological, mean-field theory that bypasses the need of knowing the microscopic aspects of the system by assuming that close to the critical temperature

1. The free energy function of the entire thermodynamic system can be expanded as a power series of a certain variable, which we will call the order parameter.

2. This function maintains the same symmetry properties of the original system's Hamiltonian.

Under Landau's theory many systems that have very different microscopic behaviors end up being described by the same free energy function, as long as their Hamiltonians

are invariant under the same transformations. This formalism was first presented by Landau in 1937 and was one of the basis for his work with Ginzburg on superconductivity. Knowing why Landau's theory works was only rigorously justified by the works of Wilson on the topic of the renormalization group, which is beyond the scope of this dissertation.

2.3.1 Order parameter

The concept of order parameter is essential to the Landau theory of phase transitions and to the phase field model, which forms the basis of the model described in this thesis. We look at this quantity as characterization of the phase of the system. The order parameter can be represented by a scalar, vector or tensor field which can, in principle, have different values at different points, i.e. is a function of position. Most of the times its value is defined such that it is null in the unordered phase and has some nonzero value in the neighboring ordered regions. Some examples of order parameter used in physics are:

- Magnetization (scalar), usually in magnetic system's such as the Ising Model.
- Magnetization (vector), for instance in the XY Model .
- When studying liquid-gas/liquid-liquid transitions the order parameter is chosen to be the difference between the densities of the two substances.
- In a Bose-Einstein condensate the order parameter is the value of the wavefunction that describes the condensate.

We see that the order parameter does not have enough information to give a detailed microscopic description of the system at hand but can be a useful measure of the global, macroscopic ordering of the system as a whole.

Another way of looking at the concept of order parameter is using a probabilistic approach. We can say that its value measures how likely it is for a neighbor of a certain point being in the same phase as itself. Ed Caruthers, a retired physicist from UT Austin gave the following explanation when asked what an order parameter is:

"The order parameter for conservatives in Texas is higher than for liberals in Texas. Statistically, a conservative in Texas is likely to have more conservative neighbors than liberal neighbors."

2.3.2 Free energy function

The first assumption that Landau made in his theory was that, near the critical point, the free energy F of the system could be written as a Taylor expansion with respect to the order parameter, ϕ. This means that near the critical point $F(\phi)$ has the form

$$F = a_0 + \sum_{n=1}^{\infty} \frac{a_n}{n} \phi^n \tag{2.10}$$

From the second assumption, F must obey the same symmetry operations as the Hamiltonian. To visualize what this means, let us construct the free energy that describes the Ising model for ferromagnetism. In this case, $\phi \equiv M$ and since the Hamiltonian is invariant under a sign exchange of the spin, it follows that

$$a_{2k+1} = 0 \quad \text{where } k = 0, 1, 2, 3, \ldots$$

To find the values of the order parameter that minimize the free energy, we have to find the solutions to

$$\frac{\mathrm{d}F}{\mathrm{d}\phi} = a_2\phi + a_4\phi^3 + a_6\phi^5 + \cdots = 0$$

and if we set that $F = 0$ when $\phi = 0$, we set $a_0 = 0$.

Bearing these condition in mind, one possible shape for F in the context of the Ising model is

$$F(\phi) = \frac{a_2}{2}\phi^2 + \frac{a_4}{4}\phi^4 \tag{2.11}$$

Minimizing this free energy we get

$$a_2\phi + a_4\phi^3 = 0$$

Its solutions are

$$\phi = 0 \vee \phi = \pm\sqrt{-\frac{a_2}{a_4}}$$

and we can see that depending on the value of a_2 and a_4, the equation either has two or no real nonzero solutions. If a_2 and a_4 are both positive, then $\phi = 0$ is the only minima of the system and there will be no two coexisting phases. For them to coexist, we require that $a_2 < 0$ while a_4 must also be positive since we do not want the system to be minimized by $\phi = \infty$, for we are looking for finite equilibrium states.

Due to the dependence of the number of equilibrium states on the sign of a_2, we can associate it with the reduced temperature of the system, meaning

$$a_2 = a_2^0 \frac{T - T_c}{T_c}$$

where a_2^0 is a positive number. In the Ising model, above T_c, $a_2 > 0$, therefore the system has zero magnetization since it is the only stable state. However, when $T < T_c$, $a_2 < 0$ and a spontaneous non-zero magnetization arises.

We can also try and find out how a_4 depends on the temperature. Writing it as a Taylor series around T_c and keeping only first order terms we get

$$a_4 = a_4^0 + a_4^1(T - T_c)$$

and since we are working very close to the critical temperature the linear term vanishes and we are left with $a_4 = a_4^0$.

Thus, below T_c the two stable values of ϕ can be written as

$$\phi \approx \pm\sqrt{\frac{a_2^0}{a_4^0}\frac{(T_c - T)}{T_c}}$$

A representation of the free energy for both positive and negative values of a_2 is presented in Figure 2.1.

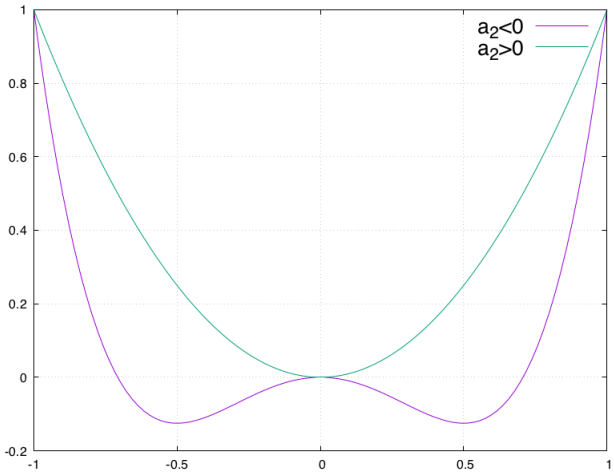

Figure 2.1: Shape of a double well function when $a_2 > 0$ (purple) and $a_2 \leq 0$ (green).

A free energy with this particular expression will be relevant in this work in the following sections.

Other functionals are used to describe different physical systems

- $H \neq 0$ Ising Model:

$$F(\phi) = a\phi^2 + b\phi^4 - H\phi$$

  In this case the nonzero magnetic field breaks the symmetry of the system, meaning that $F(\phi) \neq F(-\phi)$.

- For systems that exhibit a tricritical point, a proper free energy function is

$$F(\phi) = \frac{1}{2}a\phi^2 + \frac{1}{4}b\phi^4 + \frac{1}{6}c\phi^6 - h\phi$$

  .

2.3.3 Spinodal decomposition

Suppose we have a homogeneous mixture of two fluids A and B at a certain temperature. As we bring the mixture down to lower temperatures we start to see the formation of well defined domains of both fluids. This phenomenon is called spinodal decomposition

and this domain formation will occur until there is a single cluster of fluid A and another one of fluid B.

If we calculate the second derivative of our free energy function and make it equal to zero we get the so called spinodal line. In the case of a free energy like 2.11 we get

$$\frac{\mathrm{d}^2 F}{\mathrm{d}\phi^2} = 0 \Leftrightarrow \phi^2 = -\frac{a_2}{3a_4} = -\frac{a_2^0}{3a_4^0}(T - T_c) \tag{2.12}$$

or, if our initial state corresponds to $\phi \equiv \phi_0$

$$T = T_c - \frac{3a_4}{a_2}\phi_0^2 \tag{2.13}$$

What this condition means is that if $T < T_c - \frac{3a_4}{a_2}\phi_0^2$ the system will be unstable to small fluctuations around the minimum energy state and spinodal decomposition will occur.

2.4 Phase field model

Note: Based on [27] and [30].

The idea behind a phase field model is the introduction of an auxiliary scalar field $\phi(\vec{r}, t)$ that takes on values between two defined numbers, each representing a different phase of the system. This field is usually the order parameter, borrowing the term from Landau's theory of phase transitions.

For example, to describe an alloy that consists of an heterogeneous mixture of two metals, A and B, we can use a phase field variable that has the value -1 inside a domain of metal A and $+1$ when in a cluster of metal B. On the transition zone between a cluster of metal A and another one from B, i.e. the interface, the order parameter has a value close to 0.

Phase field models have gained popularity when modeling systems where there is phase separation and the formation of domains, for it bypasses the need of defining boundary conditions at the interface and the necessity of its tracking. Some areas where these models have been applied are fracture in materials ([31]), dendritic growth ([32]) and alloy solidification ([33]). Lately, the use of phase field models in studying biological

systems has increased, specifically in blood vessel growth ([34],[35], [36]), multicelular systems ([37]) and tumor growth.

Normally, in order to describe a mixture of two components we would use a set of differential equations that would tell us how the domains evolve with time. As those clusters expand or shrink, the interface that separates the two phases changes its shape and at each step we would have to apply boundary conditions describing the balance of concentration of each substance at that same interface. This forces us to keep track of that separation layer which is not an easy task, since it can take any shape imaginable. These models are usually referred to as *sharp interface models*.

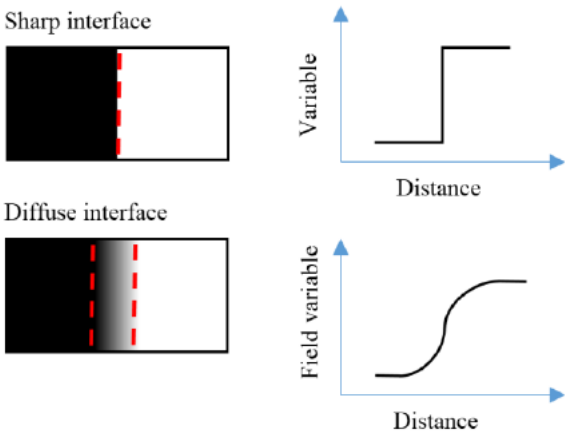

Figure 2.2: Distinction between a diffuse and sharp interface model [38].

The idea behind a phase field model is to relieve us of this need of keeping track of the interface and applying boundary conditions, by substituting the sharp interface by a diffuse interface of a certain width (Figure 2.2) and so we are in the presence of a *diffuse interface model*. The way this is done is by introducing the order parameter field that varies smoothly and continuously from one phase to the other. This way we do not need boundary conditions since, technically, there is no boundary!

The Landau framework, as discussed above, can be used to construct a dynamical model of these diffuse interface, as we discuss below. In this dynamical model we will see that a sharp interface is just a particular case of a diffuse problem when the width

of the interface layer ϵ goes to zero. In this limit, we are back at the original problem. This means that as long as we choose the value of ϵ not to be very large, we do not stray too far from our objective.

Before showing how we can build a phase field model, it is important to distinguish this theory from Landau's. First, the order parameter has different interpretations depending on the model. In Landau's theory, the order parameter has a physical meaning related to the system we are studying (magnetization, for example). In the context of phase field models, ϕ is nothing more than an identification tag for each of the phases and we do not necessarily have to attribute a meaningful interpretation to it.

Secondly, while in Landau's theory we are dealing with a thermodynamic system where its behavior is dependent on the temperature and there are fluctuations due to thermal noise, in phase field models we are only interested on the dynamics of the interface and the behavior of the bulk at different temperatures is somewhat ignored. We assume, however, that the system we are studying is at sufficiently low temperature for domain formation to occur (spinodal decomposition).

2.4.1 Free energy functional

The key step when building a phase field model is to write a free energy functional that depends on the order parameter, $F[\phi(\vec{r},t)]$, and contains information about all the physical properties and interactions relevant to the interface dynamics description.

For the phase field model to make sense, the free energy functional must include a term that takes into account the co-existence of the two distinct phases in the system and the creation of an interface between them. Usually this term is written in the following form

$$F_{\mathrm{CH}}[\phi(\vec{r},t)] = \int \left[f_0(\phi) + \frac{\epsilon^2}{2}|\nabla\phi|^2 \right] \mathrm{d}\vec{r} \tag{2.14}$$

The $\boldsymbol{\nabla}\phi$ is simply a way to energetically penalize the creation of new interface i.e. points where the spatial variation of the scalar field is non zero. This term gives rise to a surface tension in the model. In the expression, the parameter ϵ is related to the width of the interface.

Next we need to tell the system that it has two different states where its energy is minimal, so that it eventually settles into one of them. A possible form for this energy is the double-well potential borrowed from the Landau theory of phase transitions

$$f_0(\phi) = a + \frac{a_2}{2}\phi^2 + \frac{a_4}{4}\phi^4 \tag{2.15}$$

Now that a basic free energy for an interface driven by surface tension is written we can build upon it and include other terms closely related to the nature of the system. These terms can be due to applied external forces, elastic interactions, etc.

2.4.2 Cahn–Hilliard equation

Finally, we can derive an equation that tells us how the domains and the interface evolve with time, or more simply, how ϕ evolves with time. One way to find that equation is to say that the order parameter is neither created or destroyed, it is invariant, which leads to a conservation law similar to the one we find in classical electrodynamics

$$\frac{\partial \phi}{\partial t} + \boldsymbol{\nabla} \cdot \vec{J} = 0 \tag{2.16}$$

In electrodynamics, however, it is easy to know the physical meaning of $\vec{J}$, since we can directly identify it as the electric current. Here, the current of ϕ is driven by the system's free energy functional 2.14.

$$\vec{J} = -M \boldsymbol{\nabla} \mu$$

where M is a mobility/diffusion function. We can define the chemical potential (μ) of the system as the functional derivative of the free energy

$$\mu = \frac{\delta F}{\delta \phi}$$

that tells us how the free energy varies when the domains move and change their shape.

Plugging the current into (2.16) we arrive at the so called Cahn–Hilliard equation

$$\frac{\partial \phi}{\partial t} = \boldsymbol{\nabla} \cdot \left(M \boldsymbol{\nabla} \frac{\delta F}{\delta \phi} \right) \tag{2.17}$$

that allows us to study the dynamics of the order parameter. We can see that the equation has the form of a diffusion equation which is a well know parabolic partial differential equation.

In the case when M is a constant or a function of time, (2.17) simplifies to

$$\frac{\partial \phi}{\partial t} = M\nabla^2 \frac{\delta F}{\delta \phi}$$

The CH equation does not have an analytical solution and we must employ numerical integration methods that work on PDEs.

One of the systems that is accurately described by the CH equation is binary mixtures where spinodal decomposition occurs. If the system's free energy is a double well potential, its dynamics is given by the Cahn–Hilliard equation with the form

$$\frac{\partial \phi}{\partial t} = \nabla^2 \left[-\phi + \phi^3 - \epsilon^2 \nabla^2 \phi \right] \tag{2.18}$$

To show the occurrence of spinodal decomposition we can simulate a system whose initial order parameter distribution is random. At every site, the field value when $t = 0$ was chosen from a gaussian distribution centered at $\langle \phi \rangle = 0$ and with a width of $\sigma_\phi = 0.1$. The laplacian terms were calculated using a finite-difference scheme and equation 2.18 was then integrated numerically using a FTCS method (described in the appendix section) with periodic boundary conditions. In Figure 2.3 we can follow the evolution of the order parameter field and clearly see the formation of distinct domains. If we continued the simulation for a long time, we would eventually get two single domains, one for each phase.

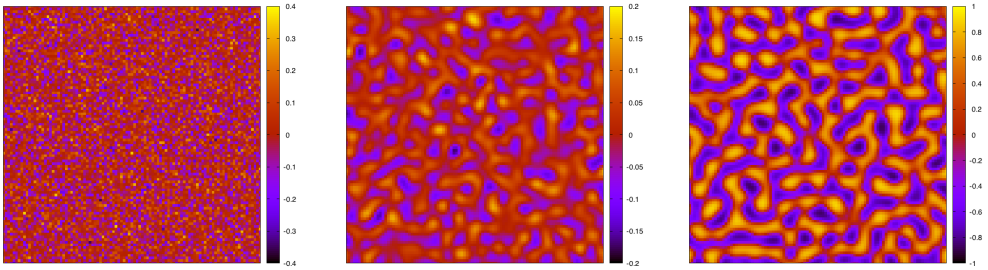

(a) (b) (c)

Figure 2.3: Evolution of a system under the Cahn–Hilliard equation. (a) $t = 0$ (b) $t = 500$ (c) $t = 3000$.

2.4.3 Other phase field models

The formalism we just described, where the order parameter is a conserved quantity, gives rise to the so called *Model B* and the dynamics is given, as we showed, by the CH equation.

Two other models are also used

- *Model A*

  In this model, the total quantity of ϕ can vary with time and the evolution equation is

  $$\frac{\partial \phi}{\partial t} = -M \frac{\delta F}{\delta \phi}$$

  and it is called the Allen–Cahn equation.

- *Model C*

  This kind of phase field model is more complicated than the previous two, since it is used on systems where the order parameter is not enough to describe the whole system and additional variables are used, giving rise to extra coupled equations. These variables can describe things like the density of impurities in a solid, acting as a second order parameter with its own dynamical equation.

Chapter 3

Model implementation

Now that all of the basic biological, physical and mathematical concepts have been explored, it is time to introduce the actual model we created to study sprouting angiogenesis. The work presented is based on the one described in the article "The Force at the Tip - Modelling Tension and Proliferation in Sprouting Angiogenesis" ([36]) and it aims at adding more complexity to its description in order to better approximate it to the biological system.

The first part of this chapter is dedicated to the process of building the free energy functional that describes the system and how we can derive a set of partial differential equations that govern its evolution. After that we show how we include tip cell traction forces, VEGF signaling and other mechanisms important in angiogenesis.

3.1 State of the art

Before describing our phase field model of sprouting angiogenesis, let us take a look at what other options exist when modeling this particular biological system.

3.1.1 Continuous models

Phase field models are included in the category of continuous models and the basic idea behind them is to derive a set of equations (usually PDEs) that tell us how the

system will evolve with time. In this type of model we avoid an individual description of the endothelial cells and study the dynamics of the bulk material. Anderson and Chaplain ([39]) were some of the first people to create a continuous model of angiogenesis, using a diffusion model to study the movement of endothelial cells. In their model, this movement was influenced by chemical factors like VEGF, haptotaxis (directed by the gradient of adhesion factors) and it presented a random behavior.

Over the years many continuous models have been developed to study angiogenesis in different contexts, such as tumor growth and wound healing, as well as in different scales i.e. single cell, multicellular, networks and tissues.

3.1.2 Cellular Potts models

Another popular method of simulating the growth of new vessels is by using a discrete model known as Cellular Potts model. Here, cells are modeled individually as groups of lattice points that have a common identifier tag and the dynamics of the system is based on the minimization of an Hamiltonian function, through the use of Monte–Carlo methods and the Metropolis–Hastings algorithm.

The Cellular Potts model was proposed by James Glazier and François Graner, who took a well known model from statistical mechanics used to study magnetic systems (called the Potts model) by setting an energy cost for variations of volume of domains, relative to a target value, and applied it to the study of cell systems.

Since then, people have used CPMs in the context of angiogenesis, notably Roeland Merks who has numerous articles published on the topic, including some with James Glazier ([40], [41], [42]).

3.2 Constructing the free energy

The first and perhaps most important step in building our model is writing an appropriate free energy functional that accounts the relevant physical details that are relevant to the interface motion. In our case, the free energy will be composed of two

parts

$$F = F_{\text{CH}} + F_{\text{mech}}$$

F_{CH} is the energy that describes phenomena related to interface creation, phase separation and surface tension. It is the term we usually associate with the standard Cahn-Hilliard equation for a binary mixture and in this model it has the form

$$F_{\text{CH}} = \int \rho_\phi \left(f_0 + \frac{\epsilon^2}{2} (\nabla\phi)^2 \right) \mathrm{d}\vec{r} \tag{3.1}$$

where

$$f_0 = -a\frac{\phi^2}{2} + \frac{\phi^4}{4} \tag{3.2}$$

and ρ_ϕ is a scale factor that controls the balance between the surface tension term (this one) and the elastic term in the free energy. Since in this model we want the system's dynamics to be driven by the elastic energy term, we should use a value for this parameter high enough for the interface to be stable but not so high as to not let the Cahn–Hilliard energy term obfuscate the mechanical contribution. An analysis of this kind of potential and the meaning of the parameter a was already done when describing Landau's theory. If we solve the Cahn–Hilliard equation simply with this free energy term we get results similar to the ones obtained in spinodal decomposition.

The second term in the free energy, F_{mech}, is the one that contains all of the contributions related to mechanical interactions in the system and can be further decomposed into

$$F_{\text{mech}} = F_{\text{ela}} + F_{\text{cell}}$$

where F_{ela} is the energy that arises from the elastic interactions between the various parts of the system and F_{cell} is the energy that comes from the force exerted by the cells on the surrounding tissue and ECM.

F_{ela} is written as the direct product of the strain and stress tensors

$$F_{\text{ela}} = \int \frac{1}{2}\sigma_{ij}\varepsilon_{ij}\mathrm{d}\vec{r} \tag{3.3}$$

and, considering that the vessel and ECM parts of the system are both homogeneous and isotropic, the strain tensor elements can be calculated using

$$\varepsilon_{ij} = \frac{1}{2}\left(\frac{\partial u_i}{\partial x_j} + \frac{\partial u_j}{\partial x_i}\right)$$

where u_i are the components of the displacement vector, and Cauchy's relation holds true

$$\sigma_{ij} = K\delta_{ij}\varepsilon_{kk} + 2\mu\left(\varepsilon_{ij} - \frac{1}{d}\delta_{ij}\varepsilon_{kk}\right)$$

Plugging in the tensor definitions into the expression for the elastic energy we arrive at

$$F_{\text{ela}} = \int \frac{1}{2}\left[\left(K - \frac{2\mu}{d}\right)\partial_i u_i \partial_j u_j + \mu\left[(\partial_i u_j)^2 + \partial_i u_j \partial_j u_i\right]\right] \mathrm{d}\vec{r} \tag{3.4}$$

We write the free energy associated with the force exerted by the cells as

$$F_{\text{cell}} = -\int \chi \boldsymbol{\nabla} \cdot \vec{u}\ \mathrm{d}\vec{r} \tag{3.5}$$

and later, we will relate the χ function with the force density exerted by the cells.

Altogether, the total mechanical energy's expression is

$$F_{\text{mech}} = \int \frac{1}{2}\left[\left(K - \frac{2\mu}{d}\right)\partial_i u_i \partial_j u_j + \mu\left[(\partial_i u_j)^2 + \partial_i u_j \partial_j u_i\right] - \chi \partial_i u_i\right] \mathrm{d}\vec{r} \tag{3.6}$$

We can write μ and K as a linear function in ϕ, such that

$$\begin{aligned} \mu &= \mu_0 - \mu_1 \phi \\ K &= K_0 - K_1 \phi \end{aligned} \tag{3.7}$$

and where the constants μ_0, μ_1, K_0 and K_1 are defined as

$$K_0 = \frac{K_{\text{ECM}} + K_{\text{EC}}}{2} \qquad \mu_0 = \frac{\mu_{\text{ECM}} + \mu_{\text{EC}}}{2}$$

i.e. they represent the average compressibility and rigidity of the system, while K_1 and μ_1 represent half the difference in the value of those two parameter between the ECM and vessel phase.

$$K_1 = \frac{K_{\text{ECM}} - K_{\text{EC}}}{2} \qquad \mu_1 = \frac{\mu_{\text{ECM}} - \mu_{\text{EC}}}{2}$$

Assuming that both μ_1 and K_1 are very small compared to the average compressibility and rigidity we can write the displacement field as a perturbation series and keep only terms up to first order

- $u_i = u_i^0 + u_i^1$, such that $u_i^0 = \partial_i \omega$
- $\mu = \mu_0 - \mu_1 \phi$
- $K = K_0 - K_1 \phi$

We define the function ω as the potential for the zero order term in the displacement field's expansion and from that definition we see that

$$\boldsymbol{\nabla} \omega = \vec{u}$$

or

$$\nabla^2 \omega = \boldsymbol{\nabla} \cdot \vec{u} \tag{3.8}$$

so what $\nabla^2 \omega$ tells us is where the tip cell compresses or decompresses the surrounding tissue.

The reason why we do this expansion is that we want to be able to describe all of the interactions in the system as a function of the order parameter, including the displacements.

3.2.1 Mechanical equilibrium

Before doing some more work on the mechanical free energy we obtained, let us see what happens when we consider that the system is in a mechanical equilibrium. In order to do that, we impose that the system's free energy is invariant when the displacement field u_i suffers a small variation, meaning that

$$\frac{\delta F}{\delta u_i} = 0$$

or, since F_{CH} is solely a function of the order parameter and independent of the displacement field

$$\frac{\delta F_{\mathrm{mech}}}{\delta u_i} = \frac{\delta F_{\mathrm{ela}}}{\delta u_i} + \frac{\delta F_{\mathrm{cell}}}{\delta u_i} = 0$$

Performing the functional derivative, the equilibrium condition translates into the following equation

$$\begin{aligned}\frac{\delta F_{\text{mech}}}{\delta u_i} &= -\left(K - \frac{2\mu}{d}\right)\partial_{ij}u_i - \mu\left(\partial_{ii}u_j + \partial_{ij}u_i\right) + \partial_j\chi \\ &= -\partial_j\sigma_{ij} - f_j\end{aligned} \tag{3.9}$$

where the last equation comes from the equilibrium condition (2.2.3) we discussed in the elasticity section of the thesis. Looking at this expression we can try to interpret the meaning of the function χ. Since

$$\partial_j\chi = -f_j$$

i.e. we see that χ is the potential associated with the force field

$$\vec{f} = -\boldsymbol{\nabla}\chi \tag{3.10}$$

Plugging in the above perturbative expansions into equation (3.9) and keeping only the lowest order terms we get

$$\begin{aligned}\frac{\delta F_{\text{mech}}}{\delta u_i^0} &= -\left(K_0 - \frac{2\mu_0}{d}\right)\partial_{ij}u_i^0 - \mu_0\left(\partial_{ii}u_j^0 + \partial_{ji}u_i\right) + \partial_j\chi \\ &= \partial_j\left[-\left(K_0 - \frac{2\mu_0}{d}\right)\partial_{ii}\omega - 2\mu_0\partial_{ii}\omega + \chi\right]\end{aligned}$$

We arrive at a Poisson equation for the function ω

$$\nabla^2\omega = \frac{\chi}{L_0} \tag{3.11}$$

where we can define $L_0 = K_0 - \frac{2\mu_0}{d} + 2\mu_0$.

3.3 Mechanical forces

As we saw, χ is a function from which the forces applied to the system can be derived. In our case we write that function as the sum of a cell-cell adhesion term χ_a and a term that comes from the traction forces, χ_t so that

$$\chi = \chi_a + \chi_t \tag{3.12}$$

The adhesion term has the simple form

$$\chi_a = -\alpha\phi$$

meaning its value will be $-\alpha$ inside the endothelial cell phase and α in the ECM. The adhesion force associated with this energy is, according to 3.10

$$\vec{f_a} = \alpha\boldsymbol{\nabla}\phi \tag{3.13}$$

and it represents the tendency endothelial cells have to stick together.

In turn, χ_t is defined such that

$$\boldsymbol{\nabla}\chi_t = -\vec{f_{\mathrm{t}}}$$

however, since it is easier to solve a single scalar equation than two equations, one for each component, we write it as

$$\nabla^2\chi_t = -\boldsymbol{\nabla}\cdot\vec{f_{\mathrm{t}}} \tag{3.14}$$

a simpler Poisson equation.

After describing the forces we can rewrite equation 3.11 as

$$\nabla^2\omega = \frac{-\alpha\phi + \chi_t}{L_0}$$

3.4 Mechanical free energy

We will now apply the same perturbation expansion to the expression for the mechanical energy. If we do that, we can write it as the sum of a zeroth and first order free energy

$$F_{\mathrm{mech}} = F^0_{\mathrm{mech}} + F^1_{\mathrm{mech}}$$

After some lengthy calculations (presented in the appendix section) we arrive at

$$F_{\mathrm{mech}} = -\int\left\{\frac{\chi^2}{2L_0} + \phi\left[\frac{1}{2}\left(K_1 - \frac{2\mu_1}{d}\right)\left(\nabla^2\omega\right)^2 + \mu_1\partial_{ij}\omega\partial_{ij}\omega\right]\right\}\mathrm{d}\vec{r} \tag{3.15}$$

Adding the Cahn–Hilliard term we had before, we finally have the complete free energy functional

$$\begin{aligned} F = -\int \Bigg\{ \rho_\phi \left(-a\frac{\phi^2}{2} + \frac{\phi^4}{4} + \frac{\epsilon^2}{2}\left(\nabla\phi\right)^2 \right) + \frac{\chi^2}{2L_0} + \\ + \phi\left[\frac{1}{2}\left(K_1 - \frac{2\mu_1}{d} \right)\left(\nabla^2\omega\right)^2 + \mu_1 \partial_{ij}\omega\partial_{ij}\omega \right] \Bigg\} \mathrm{d}\vec{r} \end{aligned} \tag{3.16}$$

Using the Cahn–Hilliard equation we can determine the temporal evolution of the order parameter field only by knowing the chemical potential of the system, which is given by the functional derivative of the free energy with respect to ϕ. If we calculate it we obtain

$$\begin{aligned} \frac{\delta F}{\delta\phi} =& \rho_\phi\left[-a\phi + \phi^3 - \epsilon^2\nabla^2\phi \right] - \frac{\alpha}{L_0}\left(\alpha\phi - \chi_t\right) + \\ &+ \frac{1}{2}\left(K_1 - \frac{2\mu_1}{d} \right)\left[\frac{2\alpha\phi}{L_0}\nabla^2\omega - \left(\nabla^2\omega\right)^2 \right] - \\ &- \mu_1\left[\partial_{ij}\omega\partial_{ij}\omega - \frac{2\alpha}{L_0}\nabla^{-2}\left[\partial_{ij}\left(\phi\partial_{ij}\omega \right) \right] \right] \end{aligned}$$

where ∇^{-2} represents the inverse laplacian operator, defined as

$$\nabla^{-2}\left(\nabla^2 f\right) = f \tag{3.17}$$

We can set the value of a, such that

$$a + \frac{\alpha^2}{L_0\rho_\phi} = 1$$

and the reason why we do this is because the presence of adhesion forces in the system tends to cause an accumulation of order parameter around the vessel phase, thus reinforcing the cohesion of the endothelial tissue. As a consequence, the stable states of the system will be shifted to values different from $\phi = \pm 1$ and redefining the parameter a is the way to reset them to the intended value.

With this in mind we arrive at

$$\begin{aligned} \frac{\delta F}{\delta\phi} =& \rho_\phi\left[-\phi + \phi^3 - \epsilon^2\nabla^2\phi \right] + \frac{\alpha\chi_t}{L_0} + \\ &+ \frac{1}{2}\left(K_1 - \frac{2\mu_1}{d} \right)\left[\frac{2\alpha\phi}{L_0}\nabla^2\omega - \left(\nabla^2\omega\right)^2 \right] - \\ &- \mu_1\left[\partial_{ij}\omega\partial_{ij}\omega - \frac{2\alpha}{L_0}\nabla^{-2}\left[\partial_{ij}\left(\phi\partial_{ij}\omega \right) \right] \right] \end{aligned} \tag{3.18}$$

3.5 Tip cell force field

Let us now describe how we include mechanical forces exerted by the tip cell in the model. The traction force will be responsible for the pulling effect of the tip cell on the rest of the endothelial cells and on the surrounding ECM. We saw that this mechanical effect is given by the χ_f function defined as

$$\boldsymbol{\nabla}\chi_t = -\vec{f_{\mathrm{t}}}$$

leading to the definition presented in equation 3.14. What we need now is to find a suitable function $\vec{f_{\mathrm{t}}}$ that represents the tip cell traction force as closely as possible to the results presented in the biological introduction of this thesis, specifically the vector field in Figure 1.8.

Finding a force field that correctly mimics the one obtained from experiments is perhaps one of the hardest tasks we face when building the model. The way we do it is we reverse engineer the force by choosing a shape for the $-\boldsymbol{\nabla}\cdot f_t$ and then solve the Poisson equation to find χ. If after, we calculate the gradient of the function we just obtained, we get the corresponding force field and we can analyze the physical consequences of having a tip cell force with such a shape.

The function we use for the divergence of f_t is

$$\boldsymbol{\nabla}\cdot\vec{f_t} = \frac{A_{\mathrm{tip}}}{R_x^2+R_y^2}\left[\frac{R_x^2\left(y-y_0\right)^2+R_y^2\left(x-x_0\right)^2}{\cosh^2\zeta}+R_x^2R_y^2\left(\tanh\zeta-1\right)\right] \tag{3.19}$$

where

$$\zeta = \frac{R_x}{2}\left[\frac{(x-x_0)^2}{R_x^2}+\frac{(y-y_0)^2}{R_y^2}-1\right]$$

and R_x and R_y are the value of the cell's axis, A_{tip} is the amplitude of the force, while $(x_0,\, y_0)$ are the coordinates of the force application center.

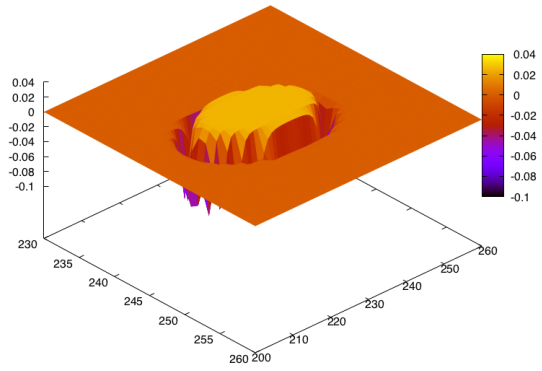

Figure 3.1: Grafical representation of $\nabla \cdot f_t$.

As we can see from the graph in Figure 3.1 the divergence of the force has practically the same value inside the cell and then the intensity drops at the border.

When we calculate the function χ_t we get the results presented in Figure 3.2. The equation is solved numerically using Fast Fourier Transforms (FFT) which automatically imposes periodic boundary conditions to the system, but we will see this has no effect on the problem when we use a large enough grid. Also, to properly define the solution to the Poisson equation we have to set the average value of the solution, and in this case we choose $\langle \chi_t \rangle = 0$.

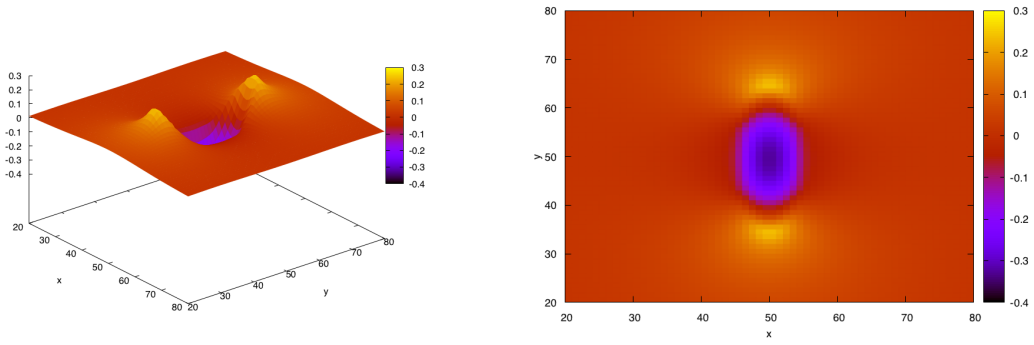

(a) 3D view.

(b) 2D top view map.

Figure 3.2: χ_f function corresponding to the force field in Figure 3.3.

The force that correspond to the χ function we just calculated is represented in Figure 3.3

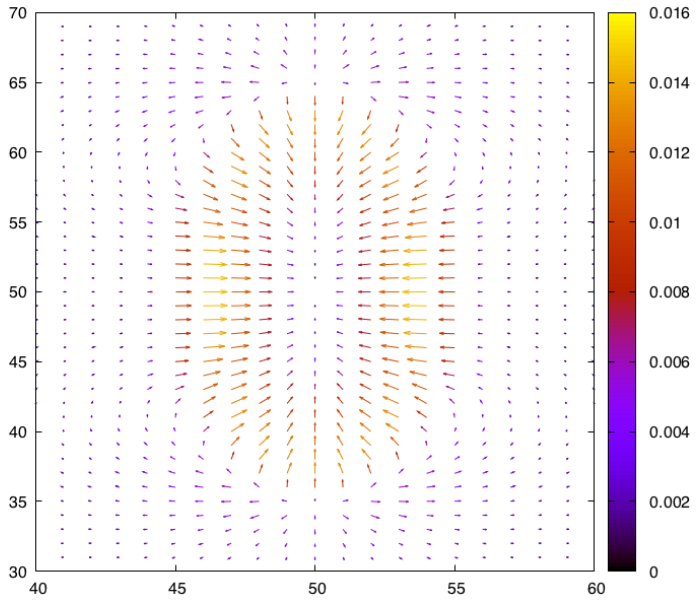

Figure 3.3: Tip cell force field

Comparing the result with the experimental measurements of an endothelial cell's force field, we see that the chosen function for the divergence of the field is able to capture some of the relevant properties. For instance, in Figure 3.3 the amplitude of the force is higher at the boundary of the cell. Also, its direction points towards the geometrical center of the ellipse.

Initially, the force is applied only in a forward direction but in reality we want the cell to move in the direction of the VEGF gradient so we have to rotate the tip cell accordingly. To do that we calculate the VEGF gradient at the grid point where we want to apply the force and then we determine

$$\begin{aligned} \cos\theta_R &= \frac{(\nabla \mathrm{VEGF})_x}{|\nabla \mathrm{VEGF}|} \\ \sin\theta_R &= \frac{(\nabla \mathrm{VEGF})_y}{|\nabla \mathrm{VEGF}|} \end{aligned} \tag{3.20}$$

where θ_R is the rotation angle. With this angle we can build the well known rotation

matrix and apply it to the coordinates of the application center

$$\begin{bmatrix} (x-x_0)' \\ (y-y_0)' \end{bmatrix} = \begin{bmatrix} \cos\theta_R & \sin\theta_R \\ -\sin\theta_R & \cos\theta_R \end{bmatrix} \begin{bmatrix} (x-x_0) \\ (y-y_0) \end{bmatrix}$$

obtaining a new set of coordinates.

There is only one more equation to solve that is related to the mechanical part of the system. What we have left to calculate is the function ω and the equation that gives its value is 3.11

$$\nabla^2\omega = \frac{-\alpha\phi + \chi_t}{L_0}$$

Since we know χ_t, calculated previously, and the other term is easily determined we can solve this equation, once again using FFT.

3.6 Solving the mechanical Cahn–Hilliard equation

To get the values of the order parameter field, ϕ, in the grid at subsequent values of time we need to solve the Cahn–Hilliard equation with the mechanical terms.

If the motility is the same for both phases the CH equation is simply

$$\frac{\partial\phi}{\partial t} = M\nabla^2\frac{\delta F}{\delta\phi}$$

and we simply need to calculate the laplacian of $\frac{\delta F}{\delta\phi}$. We can do this analytically by applying the operator to equation 3.18 and afterwards we can integrate the equation numerically.

If, however, we have a variable motility, calculating the laplacian is not enough. Since we also need the gradient of the functional derivative, we need to know the function everywhere on the grid.

The only difficulty this presents is due to the inverse laplacian operator that appears in expression 3.18. However, this is nothing more than solving another Poisson equation. If we say that

$$\nabla^{-2}\left[\partial_{ij}\left(\phi\partial_{ij}\omega\right)\right] = g$$

and apply the laplacian operator to the whole equation, we get

$$\nabla^2 g = \partial_{ij} \left(\phi \partial_{ij} \omega \right)$$

Now that we know the value of the functional derivative, what we have to do next is calculate

$$J_{i,j} = -M(\vec{r}) \left(\frac{\delta F}{\delta \phi} \right)_{i,j}$$

followed by its divergence and that gives us the complete RHS of the Cahn–Hilliard equation. After that, we simply have to integrate the equation using the FTCS method, assuming the solution has periodic boundary conditions.

This most general method is valid when M is either a constant or a function of ϕ.

3.7 VEGF dynamics

The way we model the dynamics of the vascular growth factor is by writing a reaction–diffusion equation for its concentration on the grid.

$$\frac{\partial C_V}{\partial t} = D_V \nabla^2 C_V - k_V C_V \phi \Theta(\phi) \tag{3.21}$$

where D_V is the VEGF diffusion constant, k_V its consumption rate ($k_V > 0$) and $\Theta(\phi)$ is the Heavyside function. The laplacian operator takes care of the diffusion process and is accompanied by a concentration-dependent consumption term. This last term is written such that the concentration drastically decreases when $\phi > 1$, meaning there is no VEGF inside the endothelial cells that are a part of the vessel. Since we want the tip cell to follow the VEGF gradient, if we allowed the concentration inside the endothelial tissue to have a nonzero value, the tip cell would not know where to go and the gradient at its position would probably be close to zero. By using a decay term in equation 3.21, we avoid restricting the presence of VEGF to the ECM and the need to apply zero-flux boundary conditions at the interface, which would complicate the computational implementation.

We can solve the equation for the equilibrium distribution in one dimension, which reduces to a simple decay situation (when $\phi = 1$)

$$D_V \frac{\mathrm{d}^2 C_V}{\mathrm{d}x^2} = k_V C_V$$

Its solution is well know

$$C_V = Ae^{-\sqrt{\frac{k_V}{D_V}}x} + Be^{\sqrt{\frac{k_V}{D_V}}x}$$

In order for the function to always have a finite value and for it to be zero away from the sources of VEGF, we set $B = 0$ and keep only the exponential with a negative argument

$$C_V = C_{\max} e^{-\sqrt{\frac{k_V}{D_V}}x} = C_{\max} e^{-\frac{x}{\lambda}}$$

where $C_{\max}$ is the concentration of VEGF reached at the interface. Furthermore, since the argument of the exponential must be dimensionless, we can interpret the exponent in the solution as a characteristic length λ related to the decay of C_V. If we set $x = \lambda$ we see that

$$C_V = \frac{C_{\max}}{e} \approx 0.4\ C_{\max}$$

meaning that when we are at a distance of λ from the VEGF source, the concentration has decreased by approximately 60%. We can call that length the radius of influence of VEGF

$$R_{\mathrm{VEGF}} = \sqrt{\frac{D_V}{k_V}} \tag{3.22}$$

To solve equation 3.21 we use a finite difference scheme to discretize the laplacian term, followed by integration in time using the FTCS method. The choice for the value of the diffusion constant D_V must be carefully coordinated with the choice of integration time step to avoid stability problems. At the limits of the grid we use Neumann boundary conditions, meaning there will be no growth factor gradient at the grid's boundary.

3.8 Chemotaxis

Tip cell migration occurs from places where VEGF concentration is lower to where it is higher, i.e. it follows the direction of the growth factor's gradient. In this model we do not track the position of the tip cell at every time step.

We do this because the tip cells do not exert a force on their surroundings at all time, instead they apply the force, then migrate and then reapply it after some time. Because of this, we only need to know where the tip cell is when it is time to apply the traction force once again; until then we let the system evolve freely. But how do we know where to apply the force next if we do not know where the tip cell is? All we have to do is follow the VEGF gradient starting from the previous known location of the tip cell until we reach the vessel interface. That is now the new position of the tip cell where a force will be applied.

To perform this numerically, we use a simple (yet effective) modified bissection algorithm along an axis oriented with the direction of the VEGF gradient.

While running this algorithm it is essential to know the value of ϕ evaluated at certain positions that do not belong to the grid, meaning we have to obtain this value based on the surrounding grid points. To do that we use an interpolation algorithm called bilinear interpolation (described in the appendix section) which we have found to provide a sufficiently accurate approximation with small computational cost.

Algorithm description

1. Take a small step from the position of the tip cell in the opposite direction of the VEGF gradient, to a new position x_{new}. We do this just in case the interface evolved backwards.

2. Advance in the direction of the gradient to a new position x_{new}.

3. Calculate the value of ϕ at x_{new} using the bilinear interpolation algorithm.

4. If $\phi < 0$ we have gone too far, meaning we passed the interface and reached the ECM so we reduce the stepsize by half. If $\phi > 0$ we have not yet reached the interface and are still inside the vessel so we take x_{new} as our next starting point.

5. Repeat steps 2. to 4. until the desired accuracy is obtained.

This algorithm is executed at regular intervals, more specifically, every time we want the tip cells to apply a force in the ECM.

3.9 Stalk cell proliferation

For a new sprout to remain attached to the parent vessel, stalk cells must proliferate in order to strengthen the connection to it. To include that phenomena into our model we add an extra term to the Cahn–Hilliard equation, that will then read

$$\frac{\partial \phi}{\partial t} = \boldsymbol{\nabla} \cdot \left(M \boldsymbol{\nabla} \frac{\delta F}{\delta \phi} \right) + \bar{p}(\phi) \Theta(\nabla^2 \omega + \alpha) \tag{3.23}$$

where $\bar{p}(\phi)$ is the value of the proliferation averaged on the area of the cell i.e

$$\bar{p}(\phi, C_V, \omega) = \frac{\int_\Omega p(C_V)\Theta(\phi)}{\int_\Omega \Theta(\phi)} \tag{3.24}$$

The value of function p is dependent on the VEGF concentration and on two parameters, M_p and $C_V^{\max}$, as so

$$p(C_V) = \begin{cases} \dfrac{2M_p C_V}{C_V^{\max}} & C_V < C_V^{\max} \\ 2M_p & C_V \geq C_V^{\max} \end{cases} \tag{3.25}$$

M_p limits the amount of proliferation that can occur or, in other words, how much can the order parameter ϕ locally increase. $C_V^{\max}$ corresponds to the value of local VEGF concentration necessary for the proliferation rate to reach M_p.

We should note that by adding the proliferation term to the CH equation, the amount of ϕ in the whole grid is no longer conserved.

3.10 Notch mechanism

Coupled to the continuum phase-field model described in the preceding sections, there is a small, but essential, rule that allows us to describe the process of tip/stalk cell differentiation via the Delta-Notch mechanism. This algorithm is responsible for loss of tip cell status when two cells get too close to one another.

Suppose also that we want to add a new tip cell to our system. First, new tip cells must originate from the cells around the interface. But, most importantly, we cannot put it anywhere we want since we know that tip cells that are already activated will stop their first neighbors from acquiring that phenotype so we have to choose that position taking into account where the other leading cells are located. Also, we know that the Notch mechanism is contact-dependent, so calculating the euclidean distance between the place where we are trying to place the new cell and the other tip cells may not be enough. Since this distance can be shorter than the chosen minimum but the two places may not be connected by tissue, the Notch mechanism can be ineffective. The need for a new algorithm to calculate the distance, that takes into account vessel connectivity must be found.

This kind of analysis is also important when two active tip cells get too close to each other. In this case, one of them must loose its status and revert their phenotype back to stalk cell or become quiescent.

One way to calculate the shortest distance between two places while checking for connectivity is to measure that distance along the interface of the vessel. To do that we use an algorithm created to solve mazes.

3.10.1 Maze solving algorithm

The maze solving algorithm is fairly intuitive since what it does is go to the starting point and calculate the distance from it to the neighboring points **that belong to the interface**. When we reach a point that does not belong to the interface we mark its distance as ∞ (or a very big number). If we consider first and second neighbors of the starting point, the distance will be

- First neighbors: 1
- Second neighbors: $\sqrt{2}$

Then we move on to the neighbors of the neighbors and give the value

- First neighbors of a first neighbor: $1 + 1$

- First neighbors of a second neighbor: $1 + \sqrt{2}$
- Second neighbors of a first neighbor: $\sqrt{2} + 1$
- Second neighbors of a second neighbor: $\sqrt{2} + \sqrt{2}$

and so on until we have covered all of the interface points. Since we will revisit the same points eventually, we only change their distance value if the new one is smaller than the current one.

When we are done with the entire interface, we just have to check the value of the end point to get its distance to the starting point. If it is a finite number, that means the two of them are connected and that number represents the distance. If, however, the value is ∞ that means we were not able to find a path between the two points along the interface, telling us that they are not connected.

3.10.2 Adding a new tip

The steps to add a new tip cell to the simulation are

1. Select a random interface point where we will try to place a tip cell.
2. Calculate the euclidean distance between the trial point and the other tip cells positions. If all these distances are higher than the predefined condition, the interface distance will surely be higher too and we do not need to determine it. If some are smaller, we need to do the calculation.
3. Calculate the interface distance using the maze solving algorithm. If this distance is larger for all tip cells than the set value we can add a new tip cell at the trial position.

3.10.3 Deactivating tip cells

To check if a pair of tip cells are too close for them to maintain their status, we apply the following algorithm

1. Calculate the euclidean distance between the two cells. If it is higher than the minimum distance we leave them be.

2. If, however, that distance is lower than the minimum, we calculate the distance along the interface and check again. If it is lower still, one of the tip cells must be removed.

3. We randomly choose one of the two tip cells to be deactivated.

Both these algorithms are used after the tip cells move, when they will apply a new force.

3.11 Matrix degradation

One of the improvements made on the model by Santos–Oliveira et al [36] is the possibility of ECM degradation occurring due to the existence of MMPs. Previously the motility of both the vessel and matrix phase was the same but we know that this is not true since, in reality, the ECM has a much lower mobility rate, thus presenting an obstacle for the progression of the tip cell. The inclusion of these matrixins in the model is a way to describe the behavior of the matrix more accurately, since we stop using the same mobility for both ECM and endothelial cells by saying that the mobility of the matrix is close to zero everywhere, except when in the presence of MMPs. The equation for the dynamics of its concentration is

$$\frac{\partial C_M}{\partial t} = D_M \nabla^2 C_M - k_M C_M \tag{3.26}$$

Just like the equation we presented for the VEGF concentration we have a diffusion process (laplacian term) and a decay process that is dependent on the local concentration of MMP. Also, as we did for the growth factor equation, we can define a characteristic length as

$$R_{\text{MMP}} = \sqrt{\frac{D_M}{k_M}} \tag{3.27}$$

Numerically this equation is once again solved using the FTCS integration algorithm and imposing that the function C_M goes to zero at the boundaries of the grid. Furthermore, we keep its value constant inside the TC's that at each step act as MMP sources.

The mobility function M will then have different values depending on the local value of MMP, as such

$$M(C_M) = \begin{cases} 1 & \phi > 1 \\ C_M & \phi < 2C_M - 1 \\ \frac{1}{2}(\phi + 1) & \text{otherwise} \end{cases} \tag{3.28}$$

This function sets an upper limit to the mobility of the vessel to 1 while at the same time raising it for regions of the ECM where there is a nonzero concentration of MMPs. Regions where there are no matrixins have zero mobility, meaning that locally

$$\frac{\partial \phi}{\partial t} = 0$$

according to the CH equation.

Chapter 4

Results and discussion

Finally we are in possession of a functional model capable of simulating different systems where angiogenesis occurs, and now it is time to explore its capabilities. We can also obtain useful results that shed light on the factors that influence sprouting and vessel formation.

We start by running single tip cell systems in order to fine tune the value of parameters being used in subsequent simulations and to study the migration in different conditions. Then, we move on to more complex systems with many tip cells and observe the network morphologies that are obtained while continuing to study how the differences in migratory behavior of endothelial cells can give rise to blood vessels with distinct characteristics.

4.1 Changing the mechanical properties of the system

Since we are interested in studying the influence of mechanical factors in angiogenesis, we have to find a way to change the mechanical properties of the system, meaning both ECM and endothelial tissue that forms the vessel.

When describing the model we introduced 4 parameters, μ_0, μ_1, K_0 and K_1, and we defined them in terms of the rigidity and compressibility of the ECM and endothelial cells. In truth, the value of these parameters is dependent on the Young modulus, E,

and the Poisson ratio, ν, as described in the section dedicated to the theory of elasticity

$$\mu = \frac{E}{2(1+\nu)}$$
$$K = \frac{E}{3(1-2\nu)}$$

Therefore, the input parameters we have to change are

- E_{ECM}
- ν_{ECM}
- E_{EC}
- ν_{EC}

Out of these 4 parameters we are particularly interested in varying E_{ECM}, that is what we are able to measure and control in experiments, allowing us to study the difference it has on the mechanical properties of the matrix and how it influences the migration of ECs and network formation.

Before starting to run simulations it is of paramount importance to define the appropriate units of the parameters used, so we can compare the results to experiment.

4.2 Units

For the sake of simplicity, the value of the many parameters in the model is not their real value. Instead we scale them, so that the numbers are easier to work with.

Our unit of force/pressure was set to

$$F_0 = 4.74 \times 10^3 \text{ Pa} = 4.74 \text{ kPa}$$

meaning that, for instance, an ECM with a Young modulus of $E_{\text{ECM}} = 3.0 \times 10^3$ Pa, has a value of

$$E_{\text{ECM}} = \frac{3.0 \times 10^3 \text{ Pa}}{4.74 \times 10^3 \text{ Pa}} \approx 0.6$$

in the simulation.

Since the traction force exerted by the tip cell is not constant and depends on the position (as we saw in Chapter 3), we have to find a way to measure it. If we look at the average traction force on the tip cell area as a function of the parameter we use to control the intensity of the force, we get a straight line given by the equation

$$\langle f_t \rangle = 97 \times A_{\text{tip}}$$

Because we average the force on the area of the tip cell, the result will have units of pressure so in order know the true value of the traction force we have to multiply by F_0. The value used in most of the simulation is $A_{\text{tip}} = 5 \times 10^{-4}$ which corresponds to

$$F_{\text{traction}} = 97 \times A_{\text{tip}} \times F_0 \approx 250 \text{ Pa}$$

In the model, the unit of distance is the easiest to scale since one spacing of the grid corresponds to 1μm, or

$$\Delta x = 1 = 1\mu\text{m}$$

The hardest of these conversions from scaled units to real ones, with actual meaning, was the one relating the integration step used in the simulation with the real time. To do that we simulate the migration of a single loose tip cell and calculate its velocity. We know from experiment that this velocity is more or less constant for different VEGF concentrations and has a value of 9.5 µm/hr [36]. Comparing with the the velocity we obtained in the simulation we find that

$$\Delta t = 0.02 \approx 0.2 \text{ s}$$

Since most of the simulations present in this results section ran for 10^5 time iterations, this corresponds to around 5 hours and 30 minutes. Others ran for twice that long, meaning, 11 hours.

4.3 Parameter adjustment

Before getting results for more complex systems and networks, we must choose the right set of parameters that guarantees the production of sprouts whose properties are

close to the ones observed in experiments. Since we are mainly interested in studying the effect of different mechanical properties of the ECM in vessel growth, we do not want to vary parameters that are not related to it.

In order to do that, we run the simulation for a single sprout growing in only one direction dictated by the VEGF field gradient, for different values of the adhesion coefficient α, surface tension ρ_ϕ, tip cell force amplitude A_{tip}, with no stalk cell proliferation. Also, the compressibility of both the ECM and endothelial tissue were considered the same, i.e. $K_1 = 0$, as was their mobility ($M_{\text{ECM}} = M_{EC} = 1$). Afterwards, we analyze the results in terms of **sprout shape**, **maximum migration distance** and **terminal velocity** while checking if the tip cell broke its connection to the parent vessel.

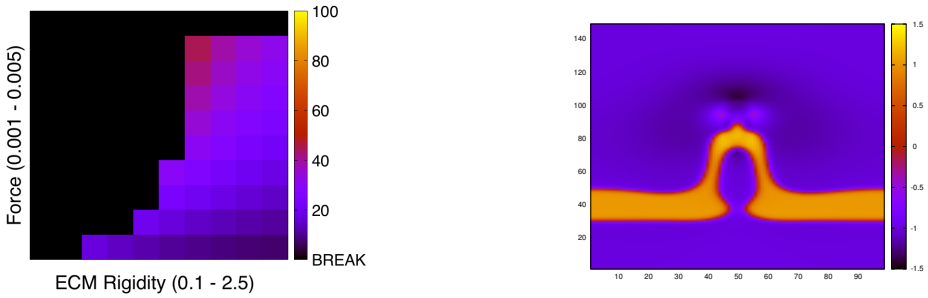

(a) $\rho_\phi = 0.1$ and $\alpha = 0.1$

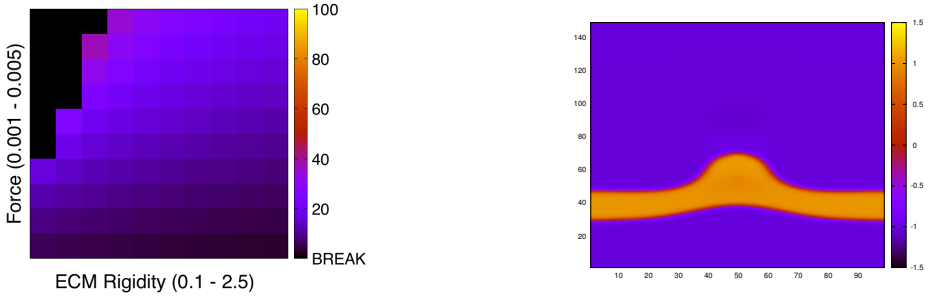

(b) $\rho_\phi = 1$ and $\alpha = 0.1$

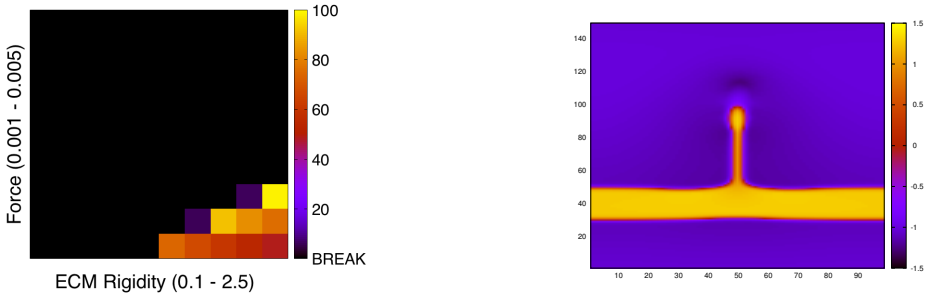

(c) $\rho_\phi = 0.1$ and $\alpha = 0.3$

Figure 4.1: Migration distance as a function of the tip cell force and the ECM rigidity and the corresponding shapes of the sprout. The ECM rigidity range goes from 0 to 2.5 and the force amplitude goes from 0.001 to 0.005. The black pixels in the phase diagrams indicate runs where the tip cell broke away from the main vessel.

In Figure 4.1 we can see migration diagrams for different values of the surface tension and adhesion parameters and the corresponding shape of the resulting sprout. Clearly we see that the parameters that give rise to the best sprout in terms of length and structure is $\rho_\phi = 0.1$ and $\alpha = 0.3$ which correspond to pictures (c). However the phase diagram does not give us much information for in this range of force amplitude the tip cell breaks in most cases. With that in mind, and in order to get more information, we simulated the same system but using less intense forces while keeping the same ρ and α, and obtained the phase diagram presented in Figure 4.2

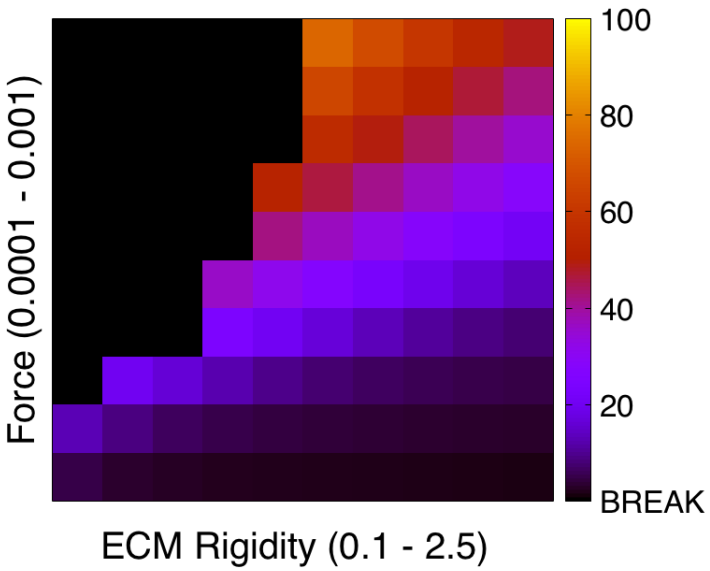

Figure 4.2: New phase diagram for less intense force amplitudes. $\rho_\phi = 1$ and $\alpha = 0.3$.

With this information we can now set a value for the surface tension and adhesion parameters, as well as for the tip cell force amplitude. From the analysis of Figure 4.2 the following values have been chosen.

- $\rho_\phi = 0.1$
- $\alpha = 0.3$
- $A_{\text{tip}} = 5 \times 10^{-4}$

Table 4.1: Value used in the simulation for some important parameters that describe the system and the corresponding physical value.

Parameter	Value	Physical Value
Grid spacing	1	1 μm
dt	0.02	0.2 s
E_{EC}	0.084	0.40 kPa
ν_{ECM}	0.13	–
ν_{EC}	0.49	–
K_{EC}	1.4	6.65 kPa
μ_{EC}	0.028	0.13 kPa
ρ_ϕ	0.1	0.47 kJ m^{-3}
α	0.3	1.42 kPa
A_{tip}	5×10^{-4}	0.25 kPa

These values guarantee the formation of sprouts with a shape close to the one we observe in experimental assays, while allowing for low rigidity regimes where the tip cell breaks and higher ones where the sprouts maintain the connection to the parent vessel.

In the next sections we vary the mechanical properties of the ECM while keeping all of the other parameters fixed (unless indicated otherwise).

4.4 Single tip cell

4.4.1 Effects of MMP on migration

One of the things we are most interested in knowing is the effect that the matrix degradation process started by the MMPs has on the migratory behaviour of the tip cells. For comparison, we first determined the migration distance of a single tip cell for different values of ECM mobility, this value being equal everywhere in it and having the value $M = 1$ for the vessel phase. The results are shown in Figure 4.3. Also, we included

in the graph a run where the action of the MMPs was taken into account.

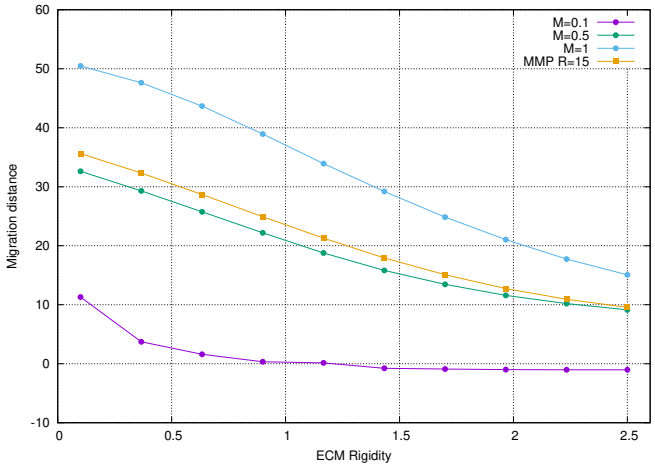

Figure 4.3: Tip cell migration distance for different values of extracellular matrix rigidity and mobility. Also one of the curves belongs to a system where MMP production by the tip cell was activated.

As expected we notice that for low mobility values (purple curve), the tip cell barely moves from its starting position. This is due to the lack of yielding from the part of the ECM that does not allow the tip cell to penetrate and advance. For higher values of M_{ECM} the tip cell is able to migrate and we see that the distance covered by it decreases as the matrix becomes more rigid. This result comes off as intuitive since the higher stiffness of the ECM leads us to expect that the tip cell will have a harder job at "drilling" through it.

We see that the run where MMP activity was modeled (with $R_{\text{MMP}} = 15$) gives similar results to when $M_{\text{ECM}} = 0.5$, although when we consider the presence of matrixins we are closer to the biological scenario we are trying to model.

After, we wanted to know how the cell migration was dependent on the radius of diffusion of the metalloproteinases so we ran the same system, changing only the value of that radius for different values of rigidity of the ECM (Figure 4.4).

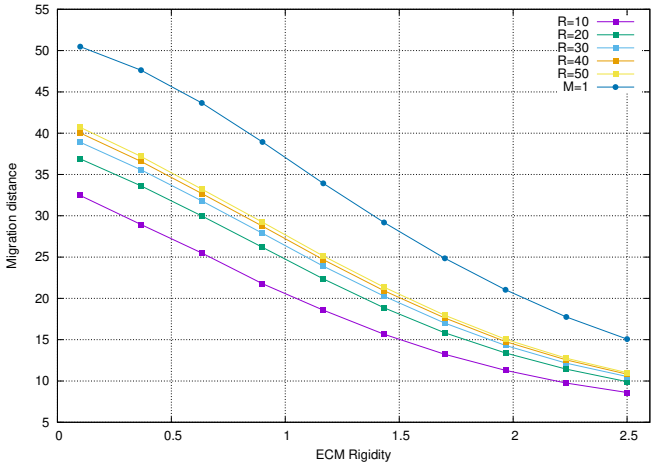

Figure 4.4: Tip cell migration distance for different values R_{MMP}. A curve with where $M = 1$ was inserted for comparison.

Here we see that increasing the range of the MMP diffusion, the tip cell is able to go further, although we also see that the difference between curves becomes smaller as the radius goes up. If the diffusion of MMP was instantaneous, we would expect that when increase the radius of action to higher and higher values, the migration curve would tend to the $M_{\mathrm{ECM}} = 1$ result. However, since the MMPs take some time to reach places far away, the motility will fall short of $M = 1$.

4.5 Multicellular systems

Now that we have studied some properties about the migration of a single tip cell, it is time to simulate multicellular systems, meaning systems where multiple sprouts start forming due to the existence of many tip cells. The system we use as a starting point is a spheroid of a certain radius emerged in a uniform VEGF distribution and on an extracellular matrix with certain mechanical properties. Also we use systems where MMPs degrade the ECM and others with constant mobility, for both the vessel and matrix phase.

4.5.1 Morphology

The first thing we can do with multicellular systems is to study how the resulting network is arranged i.e. its morphology. In systems where there are many tip cells leading the growth of new vessels, there are many possible network configurations, depending on the properties of the ECM and endothelial tissue, as well as the influence of Notch mechanism on the behavior of those same tip cells.

The starting point for these simulation are spheroids, circular shaped structures made up of endothelial cells. When placed in an environment where there are growth factors such as VEGF, the sprouting activity of these clusters is intensified and new vessels start growing radially outwards.

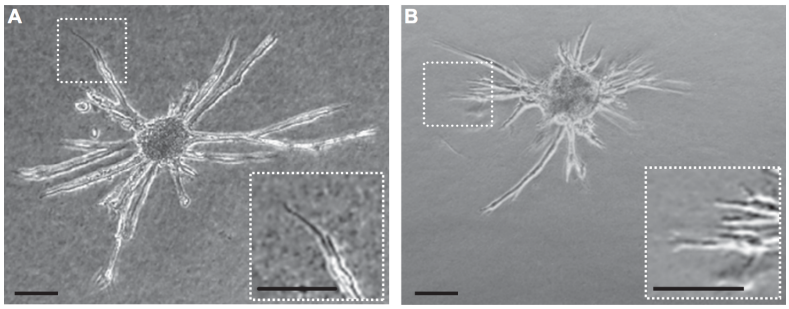

Figure 4.5: Experimental results for sprouting angiogenesis in spheroids [43].

Figure 4.5 shows two images taken in experiments where spheroids were used, where the formation of new vessels is evident ([43]).

In Figure 4.6 we have the morphologies obtained for different values of ECM rigidity. On the left column the mobility of both vessel and ECM was the same and on the right there are MMPs degrading the matrix.

We see that for low rigidity matrices, the tip cells tend to separate from the initial spheroid and migrate alone and the distance they cover is dependent on the whether there is matrix remodeling happening at the same time. For higher values of ECM rigidity, we start seeing the formation of well structured vessels that diverge from the spheroid in the radial direction. The morphology of these networks is also altered by the presence of MMPs as we see that it shortens the length of the vessels. These effects will

be seen in the following section when we present a more quantitative analysis.

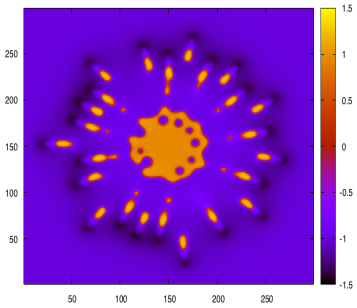

(a) $E_{\mathrm{ECM}} = 0.1$ and $M_{\mathrm{ECM}} = M_{\mathrm{EC}} = 1$.

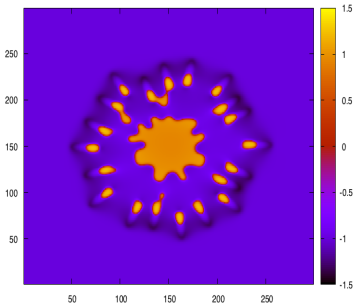

(b) $E_{\mathrm{ECM}} = 0.1$ with MMP.

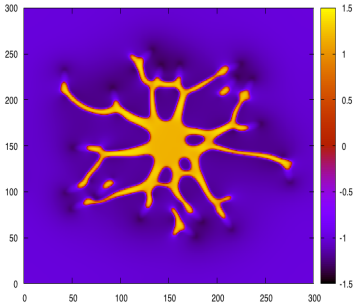

(c) $E_{\mathrm{ECM}} = 1.3$ and $M_{\mathrm{ECM}} = M_{\mathrm{EC}} = 1$.

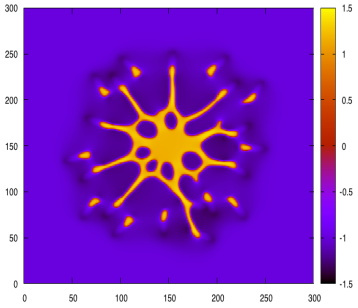

(d) $E_{\mathrm{ECM}} = 1.3$ with MMP.

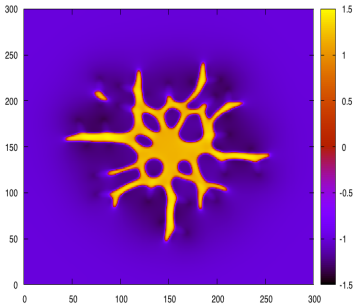

(e) $E_{\mathrm{ECM}} = 2.5$ and $M_{\mathrm{ECM}} = M_{\mathrm{EC}} = 1$.

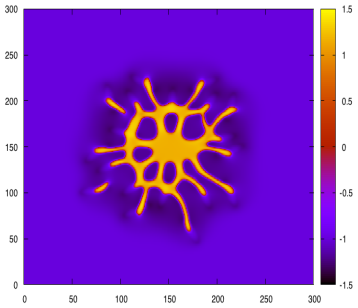

(f) $E_{\mathrm{ECM}} = 2.5$ with MMP.

Figure 4.6: Various morphologies for different values of ECM rigidity and with (left column) or without (right column) matrix remodeling.

4.5.2 Tip cell rupture

When analyzing a network, one of the things we can quantify is the number of tip cells that detach from the original spheroid and migrate alone. In Figure 4.7 we present the result of measuring that number of cells while varying the rigidity of the ECM. The data comes from running the system for a number of different seeds, since the system has a random component, specifically in the algorithms to add and remove tip cells.

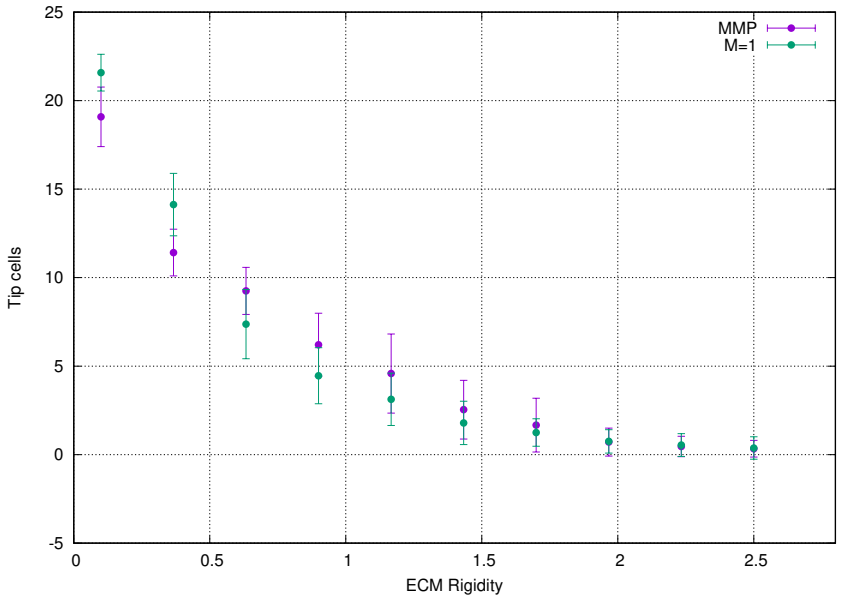

Figure 4.7: Number of loose tip cells as a function of ECM rigidity, for systems with MMPs and with constant mobility.

We see that the number of loose cells decreases as we use stiffer matrices, eventually going to zero, meaning the network maintains its integrity throughout the simulation.

Also in the same graph, we compare the same measurements for a system where both the ECM and vessel have the same mobility with a system where there is an underlying MMP field. The results do not present noticeable differences, especially when considering the error bars that go along with the data.

One place where we can look for differences between the two systems is in the average migration radius of the loose tip cells for matrices with low rigidity. If we look at Figure

4.6a and Figure 4.6b we see that the "disk" of loose tip cells has a smaller radius for systems where there is matrix degradation and larger when the mobility is the same for both ECM and endothelial tissue. The way we measure this distance and also the number of cells in Figure 4.7 is by first applying a clustering algorithm to the image and remove larger clusters that do not represent tip cells.

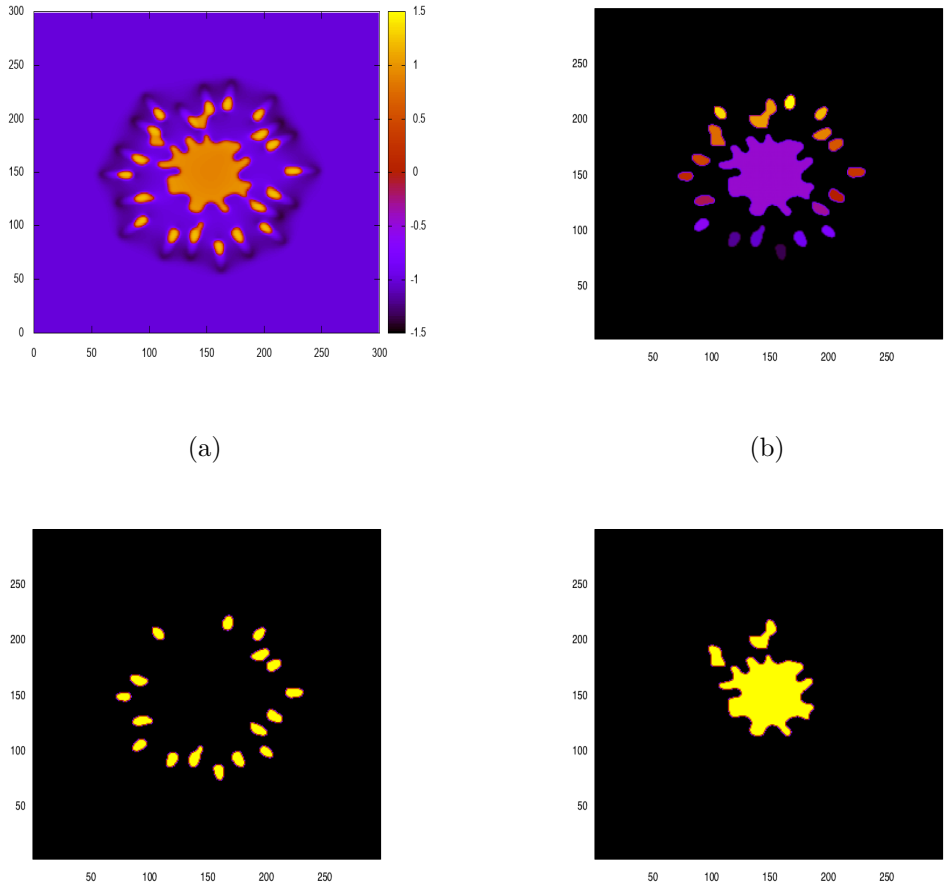

Figure 4.8: Clustering algorithm applied to a vessel network. (a) Grid to be analyzed. (b) Result of a clustering algorithm. Different clusters are marked with different colors. (c) Loose tip cells. (d) Bigger clusters.

In Figure 4.8a we have the grid we want to analyze and the first thing we do is apply

a clustering algorithm that assigns a number to each separate domain (Figure 4.8b). Then we separate the clusters by size

- Size $\leq S_{\max} \rightarrow$ Loose tip (Figure 4.8c)
- Size $> S_{\max} \rightarrow$ Cluster (Figure 4.8d)

where $S_{\max}$ is the maximum size we consider a tip cell to have. Finally we have to calculate the radial density of the order parameter, which now takes on discrete values, 1 in the vessel and 0 elsewhere. This density is calculated by generating points belonging to a circle centered at the point where the original spheroid was also centered and then calculating the value of ϕ in each of them using the bilinear interpolation algorithm.

An example of a density plot is in Figure 4.9.

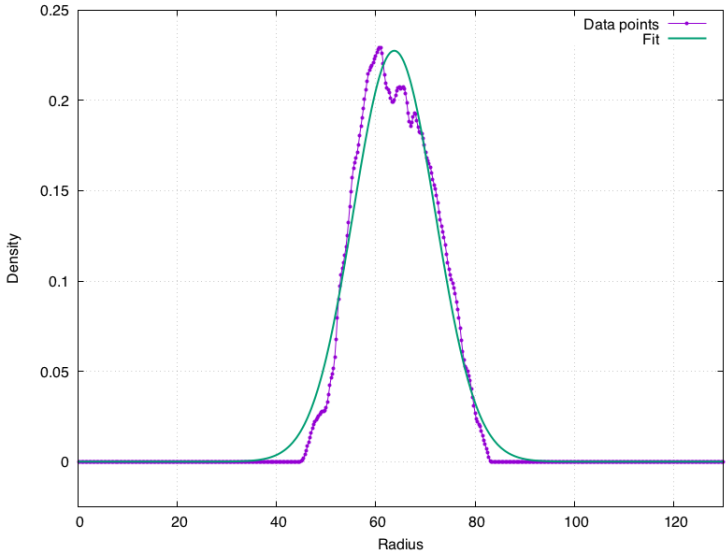

Figure 4.9: Radial density of tip cells.

We are interested in the position of the centroid of the farthest peak, which indicates that we are reaching the tip cells that have migrated further. For a more accurate determination of the position of the peak we can fit a Gaussian function using, for instance, the fitting capabilities of *Gnuplot*. Due to the width of the curve there will be some error associated with the determined x value of the maximum.

We can apply this method to grids corresponding to different ECM rigidities and see how the average migration distance varies. The results of this study are in Figure 4.10 and we see that the position of the peak does not present significant changes as we vary the stiffness of the matrix. However we clearly see that the tip cells migrate less when in the presence of MMPs and the difference in radius is ≈ 30 μm. These results were obtained only for low values of E_{ECM} for that is when most of the tip cells come loose.

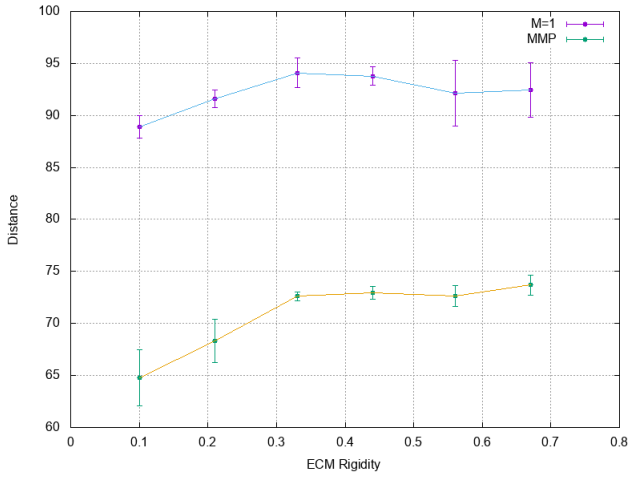

Figure 4.10: Average migration distance for different ECM rigidities, with and without ECM remodeling

For higher values of stiffness we do not have tip cells traveling alone but we have well structured vessels, as we can see in the results shown when studying the morphology of the networks. Instead of calculating the tip cell migration distance, it makes sense to measure the length of these tubular structure, and we do that also by analyzing the density of order parameter.

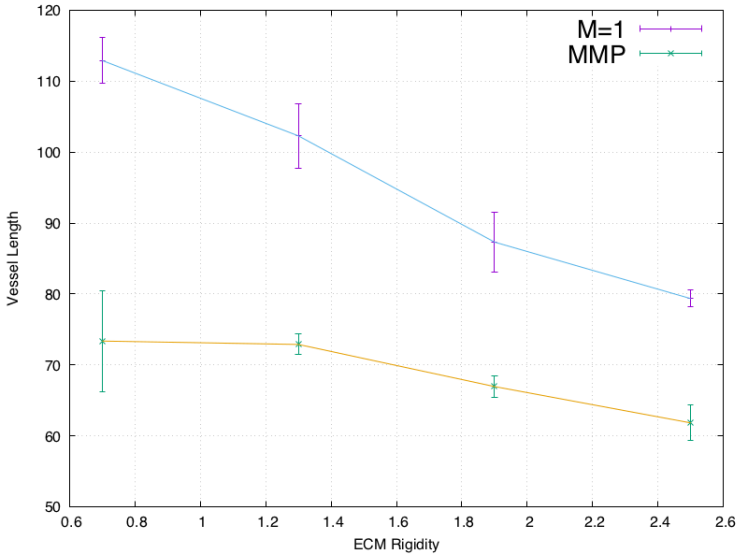

Figure 4.11: Average vessel length as a function of ECM rigidity with and without MMPs.

Analyzing the graph on Figure 4.11 we see that the average length of the sprouts gets shorter as the rigidity of the underlying matrix is higher. When comparing these results to the ones obtained for the tip cell migration distance we see that they are related. Higher stiffness, lower migration distance and shorter vessels. We also see that when matrix degradation is considered, the vessel length is also smaller than when the motility is the same everywhere on the system.

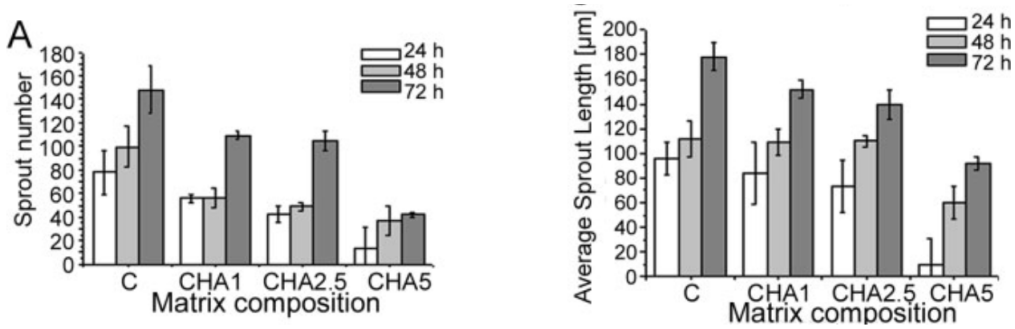

(a) (b)

Figure 4.12: Sprout number and their average length for different collagen concentrations of the ECM. By varying the concentration of collagen we can alter the matrix's rigidity [44].

Comparing the results obtained from the simulation and the experimental results in 4.12 wee see that qualitatively they are in agreement.

4.5.3 Variable compressibility

In this section we run the exact same simulations as in last section but now we introduce a small difference in compressibility between the ECM and the endothelial tissue, meaning that now $K_1 \neq 0$. In Figure 4.13, we vary the stiffness of the ECM for systems with different mobility and where $K_{\text{ECM}} > K_{\text{EC}}$. The results are presented in the next figure.

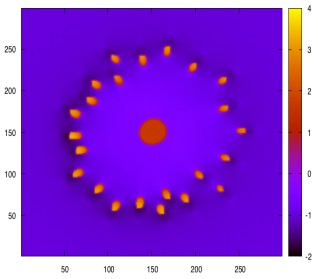

(a) $E_{\text{ECM}} = 0.1$ and $M_{\text{ECM}} = M_{\text{EC}} = 1$.

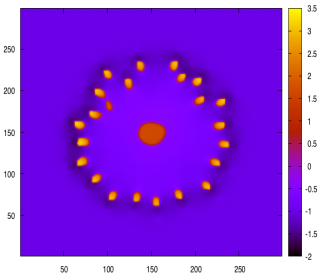

(b) $E_{\text{ECM}} = 0.1$ with MMP.

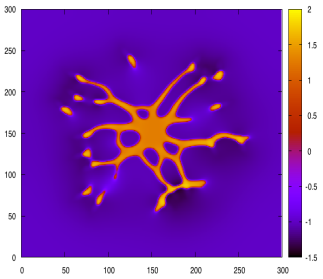

(c) $E_{\text{ECM}} = 1.3$ and $M_{\text{ECM}} = M_{\text{EC}} = 1$.

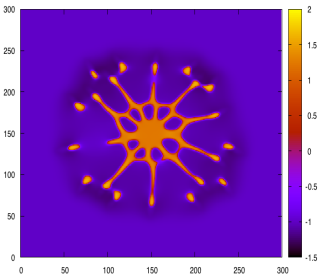

(d) $E_{\text{ECM}} = 1.3$ with MMP.

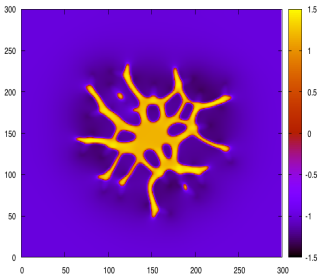

(e) $E_{\text{ECM}} = 2.5$ and $M_{\text{ECM}} = M_{\text{EC}} = 1$.

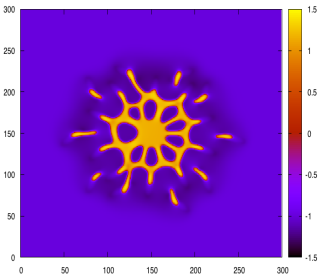

(f) $E_{\text{ECM}} = 2.5$ with MMP.

Figure 4.13: Various morphologies for different values of ECM rigidity and with (left column) or without (right column) matrix remodeling, this time with $K_1 > 0$

Comparing these results with those in Figure 4.6, we see some differences in migration, but mostly in vessel structure. Since $K_1 > 0$, the compressibility of the endothelial tissue is lower than the ECM's so the material around the area where the tip cell force is applied

tends to accumulate in that area, leading to an higher amount of ϕ. Because in these runs there is no proliferation and, consequently, the total amount of order parameter is conserved, the vessels will be thinner and the network will have more "holes".

4.5.4 Notch mechanism

To illustrate the importance of the Notch signaling pathway in the formation of new, functional, vessel networks we can simulate a system where this control mechanism is switched off. We can then compare the resulting morphology with one resulting from a normal system i.e. one where there is lateral inhibition.

The way we simulate this is simply by turning off the algorithms that regulate the addition of new tip cells to the system, and that revert the tip cell phenotype back to stalk cell when two connected tip cells are close to eachother.

In Figure 4.14 we can see the different in morphology between a system where the Notch signaling pathway is not working (in (a)) and one where it is fully working ((b)). We see that when the Notch mechanism is absent there is an abnormal high quantity of active tip cells. Also, the traction force field generated by them is superimposed, creating an excessive strain on the vessels (noticeable by the high value of ϕ in the tip cell region), which does not lead to the formation of the desired tubular structures.

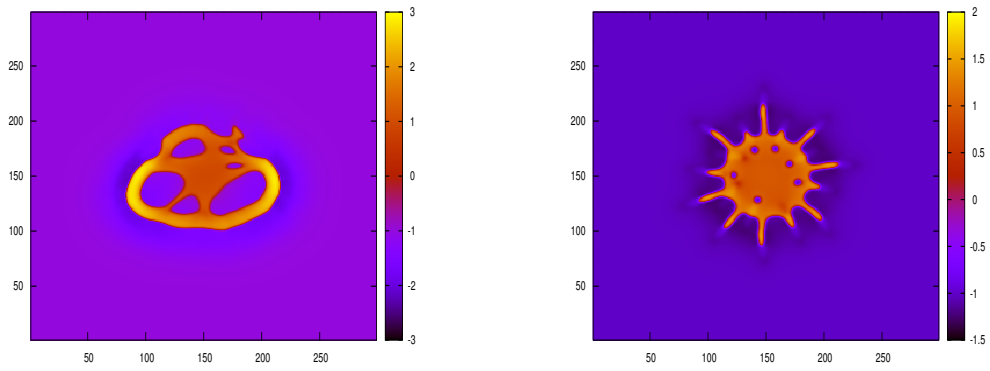

(a) (b)

Figure 4.14: Vessel network with (b) and without (a) a functional Notch mechanism.

If, however, we reinstate the Notch pathway we see the formation of regular sprouts as expected. This leads us to conclude that the existence of this control of tip cell activation is paramount to the formation of functional, healthy new blood vessels.

4.5.5 Networks

Previously, all of our simulations have focused on the sprouting activity of a single spheroid of a certain radius located at the center of the grid. Now we can see what happens when we arrange more spheroids on the grid, in order to try to obtain more complex networks, and possibly longer and thicker vessels.

The initial state of the system was the one presented in Figure 4.15a and we ran the simulation for different values of ECM rigidity. We also included ECM degradation and difference of compressibility between the matrix and the blood vessel phase, thus using the possibilities of the model to the maximum extent.

Analyzing the results in Figure 4.15 obtained for a system with multiple spheroids, we reinforce the conclusions we came to before. For ECMs with very low rigidity, we see that all of the tip cells come loose and no functional sprout capable of carrying blood is formed. For matrices with an intermediate stiffness we see that there are still some tip

cells traveling alone with no connection to the original spheroids but we already have some structure in the network. Finally, for systems where the ECM is rigid, we have barely any loose cells and the vessels organize a complex and potentially functional network with many ramifications. The organization we can see in (d) presupposes the occurrence of anastomosis, meaning many vessels merge, creating complete vessel networks.

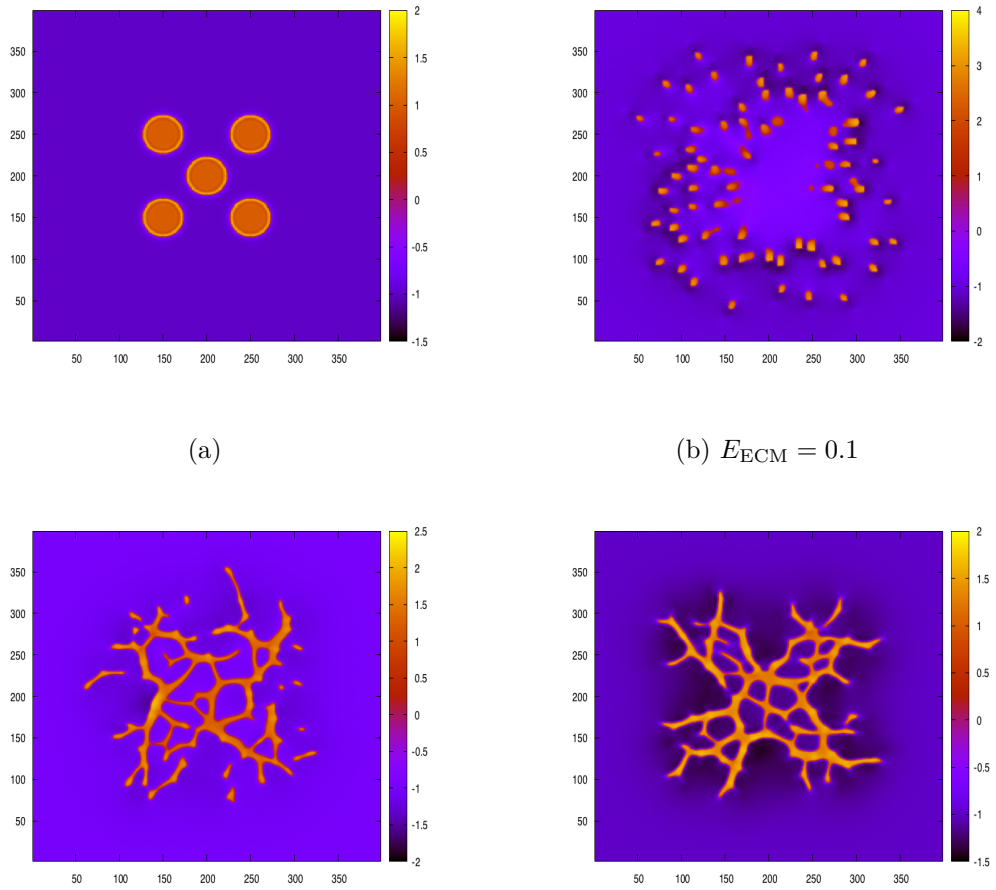

(a) (b) $E_{\mathrm{ECM}} = 0.1$

(c) $E_{\mathrm{ECM}} = 1.3$ (d) $E_{\mathrm{ECM}} = 2.5$

Figure 4.15: Vessel networks forming from a system with multiple spheroids. (a) Initial state for all simulations. (b,c,d) Structure of the network after some time, and for different ECM rigidities. These runs include ECM remodeling by MMPs.

´

Chapter 5

Conclusions and future work

By looking at the various images presented in the results we can conclude that the model described in this thesis is able to simulate and gives rise to very complex vessel networks that closely resemble the ones we see in experimental results. Also it shows that mechanical factors are indeed fundamental to the formation of these networks, in combination with the chemical signaling component.

The results obtained for various properties of the final network as a function of the ECM mechanical properties, namely its rigidity, are indicators that softer matrices with low stiffness are not ideal environments for vessel growth for they lead to the tip cells breaking away from the parent vessel. On the other hand, matrices with higher collagen concentration i.e high rigidity, lead to the possibility of sprouts elongating without breaking and even connect to one another by anastomosis.

Introducing the possibility of ECM remodeling in the system brings the description of sprouting angiogenesis made in the model closer to the real situation. It is also clear that making the ECM an obstacle to the movement of endothelial cells and then introducing the action of metalloproteases, changes the migratory potential of the tip cells, not allowing them to go as far away from their starting point.

With the inclusion of the Notch mechanism into the simulation, we have also shown that the controlled activation of new tip cells is a must if we want to be able to generate well defined and functional blood vessel networks. Otherwise, every cell will be able to

apply a traction force and the morphology of the resulting system will be abnormal.

Also, when considering differences of compressibility between the ECM and the endothelial tissue, we have seen that the resulting blood vessels are thinner than the ones we obtain by setting that difference to zero and that the amount of material accumulated in the tip cell region is higher.

On a closing note, both the model and the software where it is implemented can still be further improved, simply by taking into account more information that we can find in experimental works on angiogenesis or other studies involving the endothelial tissue and the extracellular matrix. For instance, in this work the traction force exerted by the tip cell was constant and had a fixed amplitude. This can be changed to make the force dependent on the mechanical properties of the ECM and the surrounding tissue. In this model, nothing happened inside the endothelial cells, which we know is not true. Many complex signaling pathways and reactions are occurring at the same time as the process of angiogenesis takes place and they can influence how it unfolds. These can include redox reactions involving the VEGF receptors [45], dynamics of keratin concentration near the nucleus, and other important phenomena.

Some of the fundamental factors that the presented model fails to address is the role of the blood flow in the shaping of the network. Also, in this work the VEGF concentrations on the grid where somewhat artificial, meaning they were completely controlled by the user. In reality, we know that VEGF is released by cells in need of oxygen, and these can also be included in the simulation. A model that addresses these phenomena without the mechanical interactions was developed by my colleague Maurício Moreira [46].

But perhaps the first improvement that may come to mind is upgrading this 2D model to three dimensions. This is probably not an easy task, for it will bring a much higher computational demand to the user, slowing down simulation time considerably. Some preliminary work on three dimensions was made by my colleague Hugo Ferreira in his own master's thesis [47]. A way to ease this difficulty is by rewriting the software using parallel computing techniques to profit from the full number of processors in a

laptop and especially on a cluster such as the University's own *Navigator*.

Regarding the software used to obtain the results, it is open to many improvements and optimizations when it comes to speed, memory management, and eventual bugs that have gone unnoticed so far.

Appendix A

Derivation of the model

The point of this first appendix is to show all the calculations involved in the derivation of the equations that are the backbone of this computational model.

A.1 Mechanical free energy functional

Picking up on equation 3.4 and using the definition

$$\begin{aligned}
F_{\text{ela}} &= \int \frac{1}{2}\varepsilon_{ij}\sigma_{ij} \\
&= \int \frac{1}{2}\varepsilon_{ij}\left[K\delta_{ij}\varepsilon_{kk} + 2\mu\left(\varepsilon_{ij} - \frac{\delta_{ij}}{d}\varepsilon_{kk}\right)\right]\mathrm{d}^3r \\
&= \int \frac{1}{2}\left[K\varepsilon_{jj}\varepsilon_{kk} + 2\mu\left(\varepsilon_{ij}^2 - \frac{1}{d}\varepsilon_{jj}\varepsilon_{kk}\right)\right]\mathrm{d}^3r \\
&= \int \frac{1}{2}\left[\left(K - \frac{2\mu}{d}\right)\varepsilon_{jj}\varepsilon_{kk} + 2\mu\varepsilon_{ij}^2\right]\mathrm{d}^3r \\
&= \int \frac{1}{2}\left[\left(K - \frac{2\mu}{d}\right)\partial_j u_j \partial_k u_k + \frac{\mu}{2}\left(\partial_j u_i + \partial_i u_j\right)^2\right]\mathrm{d}^3r \\
&= \int \frac{1}{2}\Big\{\left(K - \frac{2\mu}{d}\right)\partial_j u_j \partial_k u_k + \mu\left[(\partial_j u_i)^2 + \partial_i u_j \partial_j u_i\right]\Big\}\mathrm{d}^3r
\end{aligned}$$

Adding the free energy associated with the tip cell, given by 3.5, we finally get 3.6

$$F_{\text{mech}} = \int \frac{1}{2}\left[\left(K - \frac{2\mu}{d}\right)\partial_i u_i \partial_j u_j + \mu\left[(\partial_i u_j)^2 + \partial_i u_j \partial_j u_i\right] - \chi\partial_i u_i\right]\mathrm{d}\vec{r}$$

A.2 Calculating $\frac{\delta F_{\text{mech}}}{\delta u_i}$

Here we want to impose the mechanical equilibrium condition to the system, meaning

$$\frac{\delta F}{\delta u_i} = \frac{\delta F_{\text{mech}}}{\delta u_i} = 0$$

Let us calculate the functional derivative of the mechanical free energy

$$\begin{aligned} F_{\text{mec}}[u+\delta u] = \int \Big\{ & \frac{1}{2}\left(K - \frac{2\mu}{d}\right)\partial_j(u_j+\delta u_j)\partial_k(u_k+\delta u_k) + \\ & + \frac{\mu}{2}\left[(\partial_i u_j + \partial_i \delta u_j)^2 + (\partial_i u_j + \partial_i \delta u_j)(\partial_j u_i + \partial_j \delta u_i)\right] - \\ & - \chi(\partial_i u_i + \partial_i \delta u_i)\Big\} \mathrm{d}^3 r \\ = F_{\text{mec}}[u] + \int \Big\{ & \left(K - \frac{2\mu}{d}\right)\partial_j u_j \partial_k \delta u_k + \mu\left[\partial_i u_j \partial_i \delta u_j + \partial_i u_j \partial_j \delta u_i\right] - \chi \partial_i \delta u_i \Big\} \mathrm{d}^3 r \end{aligned}$$

If we perform integration by parts so that all terms are multiplied by δu_j

$$\delta F_{\text{mech}} = \int \Big\{ -\left(K - \frac{2\mu}{d}\right)\partial_{ij} u_i - \mu\left(\partial_{ii} u_j + \partial_{ji} u_i\right) + \partial_j \chi \Big\} \delta u_j \mathrm{d}^3 r$$

and according to the definition of functional derivative

$$\frac{\delta F_{\text{mech}}}{\delta u_i} = -\left(K - \frac{2\mu}{d}\right)\partial_{ij} u_i - \mu\left(\partial_{ii} u_j + \partial_{ji} u_i\right) + \partial_j \chi$$

Afterwards we write K, μ and u_i as perturbation series and arrive at equation 3.11.

A.3 Mechanical energy expansion

The complete mechanical energy of the system is written as

$$F_{\text{mech}} = \int \Big\{ \underbrace{\frac{1}{2}\left(K - \frac{2\mu}{d}\right)\partial_j u_j \partial_k u_k}_{\text{Term A}} + \underbrace{\frac{\mu}{2}\left[(\partial_j u_i)^2 + \partial_i u_j \partial_j u_i\right]}_{\text{Term B}} - \underbrace{\chi \partial_i u_i}_{\text{Term C}} \Big\} \mathrm{d}^3 r$$

In order to organize the calculations and to make them clearer, the terms in F_{mech} where labeled so we can deal with them separately. What we will do is apply the perturbation series and split the integrals into zeroth and first order terms

Term A

$$\begin{aligned}
\int \frac{1}{2}\left(K-\frac{2\mu}{d}\right)\partial_j u_j \partial_k u_k &= \int \frac{1}{2}\left[\left(K_0 - K_1\phi - \frac{2\mu_0}{d} + \frac{2\mu_1}{d}\phi\right)\right]\left[\partial_j\left(u_j^0+u_j^1\right)\partial_k\left(u_k^0+u_k^1\right)\right]\mathrm{d}^3r \\
&= \int \frac{1}{2}\left[\left(K_0-\frac{2\mu_0}{d}\right)-\left(K_1-\frac{2\mu_1}{d}\right)\phi\right]\left[\partial_j u_j^0\partial_k u_k^0 + 2\partial_j u_j^0\partial_k u_k^1\right]\mathrm{d}^3r \\
&= \int\left[\frac{1}{2}\left(K_0-\frac{2\mu_0}{d}\right)\partial_j u_j^0\partial_k u_k^0\right]\mathrm{d}^3r + \Big\}0^{\text{th}}\text{ order} \\
&+ \int\left[\left(K_0-\frac{2\mu_0}{d}\right)\partial_j u_j^0\partial_k u_k^1 - \frac{\phi}{2}\left(K_1-\frac{2\mu_1}{d}\right)\partial_j u_j^0\partial_k u_k^0\right]\mathrm{d}^3r \quad \Big\}1^{\text{st}}\text{ order}
\end{aligned}$$

0^{th} order term

$$\int \frac{1}{2}\left(K_0-\frac{2\mu_0}{d}\right)\partial_i u_i^0\partial_j u_j^0\mathrm{d}^3r = \int \frac{1}{2}\left(K_0-\frac{2\mu_0}{d}\right)\partial_{ii}\omega\partial_{jj}\omega\ \mathrm{d}^3r$$

1^{st} order term

$$\begin{aligned}
&\int\left(K_0-\frac{2\mu_0}{d}\right)\partial_i u_i^0\partial_j u_j^1\mathrm{d}^3r - \int\frac{\phi}{2}\left(K_1-\frac{2\mu_1}{d}\right)\partial_i u_i^0\partial_j u_j^0\mathrm{d}^3r = \\
=&\int\left(K_0-\frac{2\mu_0}{d}\right)\partial_{ii}\omega\partial_j u_j^1\mathrm{d}^3r - \int\frac{\phi}{2}\left(K_1-\frac{2\mu_1}{d}\right)\partial_{ii}\omega\partial_{jj}\omega\mathrm{d}^3r = \\
=&-\int\left(K_0-\frac{2\mu_0}{d}\right)\partial_{iij}\omega\ u_j^1\mathrm{d}^3r - \int\frac{\phi}{2}\left(K_1-\frac{2\mu_1}{d}\right)\partial_{ii}\omega\partial_{jj}\omega\mathrm{d}^3r
\end{aligned}$$

Term B

$$\begin{aligned}
\int\frac{\mu}{2}\left[(\partial_i u_j)^2+\partial_i u_j\partial_j u_i\right]\mathrm{d}^3r &= \int\left(\frac{\mu_0-\mu_1\phi}{2}\right)\left[\left(\partial_i u_j^0+\partial_i u_j^1\right)^2+\left(\partial_i u_j^0+\partial_i u_j^1\right)\left(\partial_j u_i^0+\partial_j u_i^1\right)\right]\mathrm{d}^3r \\
&= \int\left(\frac{\mu_0-\mu_1\phi}{2}\right)\left[(\partial_i u_j^0)^2+\partial_i u_j^0\partial_j u_i^0+2\partial_i u_j^0\partial_i u_j^1+2\partial_i u_j^0\partial_j u_i^1\right]\mathrm{d}^3r \\
&= \underbrace{\int\frac{\mu_0}{2}\left[(\partial_i u_j^0)^2+\partial_i u_j^0\partial_j u_i^0\right]\mathrm{d}^3r}_{0^{\text{th}}\text{ order}} + \\
&+ \underbrace{\int\mu_0\left(\partial_i u_j^0\partial_i u_j^1+\partial_i u_j^0\partial_j u_i^1\right)\mathrm{d}^3r - \int\frac{\mu_1\phi}{2}\left[(\partial_i u_j^0)^2+\partial_i u_j^0\partial_j u_i^0\right]\mathrm{d}^3r}_{1^{\text{st}}\text{ order}}
\end{aligned}$$

0^{th} order term

$$\begin{aligned}\int \frac{\mu_0}{2}\left[(\partial_i u_j^0)^2 + \partial_i u_j^0 \partial_j u_i^0\right]\ \mathrm{d}^3r &= \int \frac{\mu_0}{2}\left[(\partial_{ij}\omega)^2 + \partial_{ij}\omega\partial_{ji}\omega\right]\ \mathrm{d}^3r \\ &= \int \mu_0(\partial_{ij}\omega)^2\ \mathrm{d}^3r \\ &= -\int \mu_0 \partial_{ijj}\omega\partial_i\omega\ \mathrm{d}^3r \\ &= \int \mu_0 \partial_{ii}\omega\partial_{jj}\omega\ \mathrm{d}^3r\end{aligned}$$

1^{st} order term

$$\begin{aligned}&\int \mu_0\left(\partial_i u_j^0 \partial_i u_j^1 + \partial_i u_j^0 \partial_j u_i^1\right)\mathrm{d}^3r - \int \frac{\mu_1\phi}{2}\left[(\partial_i u_j^0)^2 + \partial_i u_j^0\partial_j u_i^0\right]\mathrm{d}^3r = \\ &= \int 2\mu_0\partial_{ij}\omega\partial_i u_j^1 \mathrm{d}^3r - \int \mu_1\phi(\partial_{ij}\omega)^2\mathrm{d}^3r = \\ &= -\int 2\mu_0\partial_{iij}\omega u_j^1\ \mathrm{d}^3r - \int \mu_1\phi(\partial_{ij}\omega)^2\mathrm{d}^3r\end{aligned}$$

Term C

$$-\int \chi\partial_i u_i = \underbrace{-\int \chi\partial_i u_i^0 \mathrm{d}^3r}_{0^{\text{th}}\text{ order}}\underbrace{-\int \chi\partial_i u_i^1 \mathrm{d}^3r}_{1^{\text{st}}\text{ order}}$$

0^{th} order term

$$-\int \chi\partial_i u_i^0 \mathrm{d}^3r = -\int \chi\partial_{ii}\omega \mathrm{d}^3r$$

1^{st} order term

$$-\int \chi\partial_i u_i^1 \mathrm{d}^3r = -\int \partial_i\chi u_i^1 \mathrm{d}^3r$$

Now that we have worked on the three terms of the mechanical energy and have separated them into zeroth and first order terms we can collect them and see what we obtain.

0^{th} order equation

$$\begin{aligned} F^0_{\text{mech}} &= \int \left[\frac{1}{2}\left(K_0 - \frac{2\mu_0}{d}\right)\partial_{ii}\omega\partial_{jj}\omega + \mu_0\partial_{ii}\omega\partial_{jj}\omega - \chi\partial_{ii}\omega\right]\mathrm{d}^3r = \\ &= \int \left[\frac{1}{2}\left(K_0 - \frac{2\mu_0}{d} + 2\mu_0\right)(\nabla^2\omega)^2 - \chi\nabla^2\omega\right]\mathrm{d}^3r \end{aligned}$$

Remembering the equilibrium condition

$$\nabla^2\omega = \frac{\chi}{L_0}$$

we end up with

$$F^0_{\text{mech}} = -\int \frac{\chi^2}{2L_0}\mathrm{d}^3r$$

1^{st} order equation

$$\begin{aligned} F^1_{\text{mech}} &= -\int \left[\left(K_0 - \frac{2\mu_0}{d}\right)\partial_{iij}\omega u^1_j + \frac{\phi}{2}\left(K_1 - \frac{2\mu_1}{d}\right)(\nabla^2\omega)^2 + 2\mu_0\partial_{iij}\omega + \mu_1\phi(\partial_{ij}\omega)^2 - \partial_i\chi u^1_i\right]\mathrm{d}^3r \\ &= -\int \left(L_0\partial_{iij}\omega - \partial_j\chi\right)u^1_j\ \mathrm{d}^3r - \int \left[\frac{\phi}{2}\left(K_1 - \frac{2\mu_1}{d}\right)(\nabla^2\omega)^2 + \mu_1\phi(\partial_{ij}\omega)^2\right]\mathrm{d}^3r \\ &= -\int \phi\left[\frac{1}{2}\left(K_1 - \frac{2\mu_1}{d}\right)(\nabla^2\omega)^2 + \mu_1(\partial_{ij}\omega)^2\right]\mathrm{d}^3r \end{aligned}$$

We see that the final result is independent of any component u^1_i because their coefficients obey the equilibrium equation.

Finally we have the functional that gives us the mechanical energy of the full system

$$F_{\text{mech}} = -\int \left\{\frac{\chi^2}{2L_0} + \phi\left[\frac{1}{2}\left(K_1 - \frac{2\mu_1}{d}\right)(\nabla^2\omega)^2 + \mu_1(\partial_{ij}\omega)^2\right]\right\}\mathrm{d}^3r$$

Complete functional

If we add up the mechanical energy functional to the pure Cahn–Hilliard term described above, we get

$$F[\phi] = \int \Big\{ \underbrace{\rho_\phi \left[-\frac{a}{2}\phi^2 + \frac{1}{4}\phi^4 + \frac{\epsilon^2}{2}(\nabla\phi)^2 \right]}_{F_{\mathrm{CH}}} \underbrace{-\frac{\chi^2}{2L_0}}_{F^0_{mech}} \underbrace{-\phi \left[\frac{1}{2}\left(K_1 - \frac{2\mu_1}{d} \right)(\nabla^2\omega)^2 + \mu_1(\partial_{ij}\omega)^2 \right]}_{F^1_{mech}} \Big\} \mathrm{d}^3 r$$

A.4 Functional derivative of the total free energy

For the Cahn-Hilliard equation we need the functional derivative of the free energy of the system with respect to a small variation of the order parameter ϕ.

$F_{\mathbf{CH}}$

$$F_{\mathrm{CH}}[\phi + \delta\phi] = \int \rho_\phi \Big\{ -\frac{a}{2}(\phi + \delta\phi)^2 + \frac{1}{4}(\phi + \delta\phi)^4 + \frac{\epsilon^2}{2}[\nabla(\phi + \delta\phi)]^2 \Big\} \mathrm{d}^3 r$$

Since we are assuming that the variation $\delta\phi$ is small, we will ignore every quadratic term of $\delta\phi$ or $\nabla\delta\phi$, as well as higher order terms. With that in mind we are left with

$$\begin{aligned} F_{\mathrm{CH}}[\phi + \delta\phi] &= \int \rho_\phi \Big\{ -\frac{a}{2}(\phi^2 + 2\phi\delta\phi) + \frac{1}{4}(\phi^4 + 4\phi^3\delta\phi) + \frac{\epsilon^2}{2}[(\nabla\phi)^2 + 2\nabla\phi\cdot\nabla\delta\phi] \Big\} \mathrm{d}^3 r \\ &= F_{\mathrm{CH}}[\phi] + \int \rho_\phi \left[-a\phi\delta\phi + \phi^3\delta\phi + \epsilon^2(\nabla\phi\cdot\nabla\delta\phi) \right] \mathrm{d}^3 r \\ \Leftrightarrow \delta F_{\mathrm{CH}} &= \int \rho_\phi \left[-a\phi + \phi^3 \right] \delta\phi \ \mathrm{d}^3 r + \rho_\phi \epsilon^2 \int \nabla\phi\cdot\nabla\delta\phi \ \mathrm{d}^3 r \end{aligned}$$

To get to the final result we have to perform integration by parts:

$$\int \nabla\phi\cdot\nabla\delta\phi \ \mathrm{d}^3 r = \int \nabla\phi \ \delta\phi \ \mathrm{d}^3 r - \int \nabla^2\phi \ \delta\phi \ \mathrm{d}^3 r$$

Assuming that we are dealing our system is described using periodic boundary conditions the term containing $\nabla\phi$ will vanish when integrating over the whole volume. We therefore have that

$$\delta F_{\mathrm{CH}} = \int \rho_\phi \left[-a\phi + \phi^3 - \epsilon^2\nabla^2\phi \right] \delta\phi \ \mathrm{d}^3 r$$

According to the definition of functional derivative given above, we thus have

$$\frac{\delta F_{\mathrm{CH}}}{\delta \phi} = \rho_\phi \left[-a\phi + \phi^3 - \epsilon^2 \nabla^2 \phi \right]$$

$F^0_{\mathbf{mech}}$

$$\begin{aligned} F^0_{\mathrm{mech}}[\phi + \delta\phi] &= -\int \frac{1}{2L_0} \left[-\alpha(\phi + \delta\phi) + \chi_t \right]^2 \mathrm{d}^3 r \\ &= F^0_{\mathrm{mech}}[\phi] - \int \frac{1}{2L_0} \left[2\alpha^2 \phi - 2\alpha\chi_t \right] \delta\phi \ \mathrm{d}^3 r \\ \delta F^0_{\mathrm{mech}} &= \int -\frac{\alpha}{L_0} \left(\alpha\phi - \chi_t \right) \delta\phi \ \mathrm{d}^3 r \end{aligned}$$

By the definition of functional derivative, we arrive at:

$$\frac{\delta F^0_{\mathrm{mech}}}{\delta \phi} = -\frac{\alpha}{L_0} \left(\alpha\phi - \chi_t \right)$$

$F^1_{\mathbf{mech}}$

$$\begin{aligned} F^1_{\mathrm{mec}}\left[\phi + \delta\phi\right] &= -\int (\phi + \delta\phi) \left[\frac{1}{2} \left(K_1 - \frac{2\mu_1}{d} \right) \left(\nabla^2 \omega + \nabla^2 \delta\omega \right)^2 + \mu_1 \left(\partial_{ij}\omega + \partial_{ij}\delta\omega \right)^2 \right] \\ &= -\int \phi \left\{ \frac{1}{2} \left(K_1 - \frac{2\mu_1}{d} \right) \left[(\nabla^2\omega)^2 + 2\nabla^2\omega\nabla^2\delta\omega \right] + \mu_1 \left[(\partial_{ij}\omega)^2 + 2\partial_{ij}\omega\partial_{ij}\delta\omega \right] \right\} \mathrm{d}^3 r \ - \\ &- \int \delta\phi \left[\frac{1}{2} \left(K_1 - \frac{2\mu_1}{d} \right) (\nabla^2\omega)^2 + \mu_1 (\partial_{ij}\omega)^2 \right] \mathrm{d}^3 r \\ &= F^1_{\mathrm{mec}}[\phi] - \int \phi \left[\left(K_1 - \frac{2\mu_1}{d} \right) \nabla^2\omega\nabla^2\delta\omega + 2\mu_1 \partial_{ij}\omega\partial_{ij}\delta\omega \right] \mathrm{d}^3 r \ - \\ &- \int \delta\phi \left[\frac{1}{2} \left(K_1 - \frac{2\mu_1}{d} \right) (\nabla^2\omega)^2 + \mu_1 (\partial_{ij}\omega)^2 \right] \mathrm{d}^3 r \\ \delta F^1_{\mathrm{mec}} &= -\int \phi \left(K_1 - \frac{2\mu_1}{d} \right) \nabla^2\omega\nabla^2\delta\omega \ \mathrm{d}^3 r - \\ &- \int \frac{1}{2} \left(K_1 - \frac{2\mu_1}{d} \right) \left(\nabla^2\omega \right)^2 \delta\phi \ \mathrm{d}^3 r - \\ &- \int 2\mu_1 \phi \partial_{ij}\omega\partial_{ij}\delta\omega \ \mathrm{d}^3 r - \\ &- \int \mu_1 \left(\partial_{ij}\omega \right)^2 \delta\phi \ \mathrm{d}^3 r \end{aligned}$$

Recall that ω obeys the equation

$$\nabla^2\omega = \frac{1}{L_0}\left(-\alpha\phi + \chi_t\right)$$

and since χ_t is independent of the order parameter, then:

$$\nabla^2\delta\omega = -\frac{\alpha}{L_0}\delta\phi$$

Also, if we define an inverse laplacian operator, ∇^{-2}, such that:

$$\nabla^{-2}\left(\nabla^2 f\right) = f$$

we have that

$$\delta\omega = -\frac{\alpha}{L_0}\nabla^{-2}\delta\phi$$

Using these results in the calculations above we obtain

$$\begin{aligned}
\delta F^1_{\text{mech}} = &\int \frac{\alpha\phi}{L_0}\left(K_1 - \frac{2\mu_1}{d}\right)\nabla^2\omega\delta\phi \ \mathrm{d}^3r - \\
&- \int \frac{1}{2}\left(K_1 - \frac{2\mu_1}{d}\right)\left(\nabla^2\omega\right)^2\delta\phi \ \mathrm{d}^3r - \\
&- \int \mu_1\left(\partial_{ij}\omega\right)^2\delta\phi \ \mathrm{d}^3r - \\
&- \int 2\mu_1\phi\partial_{ij}\omega\partial_{ij}\delta\omega \ \mathrm{d}^3r
\end{aligned}$$

Integrating by parts multiple times we find that the last term above, can be written as:

$$-\int 2\mu_1\phi\partial_{ij}\omega\partial_{ij}\delta\omega \ \mathrm{d}^3r = \int \frac{2\mu_1\alpha}{L_0}\nabla^{-2}\left[\partial_{ij}\left(\phi\partial_{ij}\omega\right)\right]\delta\phi\mathrm{d}^3r$$

Now, using the definition of functional derivative we arrive at:

$$\frac{\delta F^1_{\text{mech}}}{\delta\phi} = \frac{1}{2}\left(K_1 - \frac{2\mu_1}{d}\right)\left[\frac{2\alpha\phi}{L_0}\nabla^2\omega - \left(\nabla^2\omega\right)^2\right] - \mu_1\left[\left(\partial_{ij}\omega\right)^2 - \frac{2\alpha}{L_0}\nabla^{-2}\left[\partial_{ij}\left(\phi\partial_{ij}\omega\right)\right]\right]$$

All we have to do now to get the full functional derivative of the free energy is sum the three different terms

$$\begin{aligned}
\frac{\delta F}{\delta\phi} = &\rho_\phi\left[-a\phi + \phi^3 - \epsilon^2\nabla^2\phi\right] - \frac{\alpha}{L_0}\left(\alpha\phi - \chi_t\right) + \\
&+ \frac{1}{2}\left(K_1 - \frac{2\mu_1}{d}\right)\left[\frac{2\alpha\phi}{L_0}\nabla^2\omega - \left(\nabla^2\omega\right)^2\right] - \\
&- \mu_1\left[\left(\partial_{ij}\omega\right)^2 - \frac{2\alpha}{L_0}\nabla^{-2}\left[\partial_{ij}\left(\phi\partial_{ij}\omega\right)\right]\right]
\end{aligned}$$

Appendix B

Solving PDEs via Fourier Transform

While studying any problem in Physics it is almost inevitable that we come across a partial differential equation or PDE, for short. There are many methods available to find their solutions such as separation of variables, series solutions, perturbation methods, etc. Another way to solve them, either analytically or numerically is by using Fourier transforms. Let us look at the Poisson equation, one of the most recurring PDEs, specially in electrodynamics

$$\nabla^2 V(\vec{r}) = \rho(\vec{r})$$

Now we can write the solution written in an infinite basis of plane waves

$$V(\vec{r}) = \int_{\infty}^{+\infty} \tilde{V}(\vec{k}) e^{i\vec{k}\cdot\vec{r}} \mathrm{d}\vec{k}$$

and do the same to the function $\rho(\vec{r})$. Plugging them both into the equation we are trying to solve, we get

$$-\left|\vec{k}\right|^2 \tilde{V}(\vec{k}) = \tilde{\rho}(\vec{k})$$

which is an algebraic equation. Solving for $\tilde{V}(\vec{k})$ we get

$$\tilde{V}(\vec{k}) = -\frac{\tilde{\rho}(\vec{k})}{\left|\vec{k}\right|^2}$$

Now all we have to do is apply the inverse Fourier transform and we have the answer to our problem back in real space.

Appendix C

Numerical methods

C.1 Finite differences

Finite differences are the simplest way we can calculate a functions derivatives on a discrete grid and it is based on the mathematical definition of derivative as a limit

$$f'(a) = \lim_{h \to 0} \frac{f(a+h) - f(a)}{h}$$

Less rigorous is the notion of derivative as a slope

$$m = \frac{\Delta y}{\Delta x}$$

Since in numerical simulation we are dealing with discrete representations of functions in a grid of a certain spacing, we can't use the rigorous definition and must settle for an approximation. Let us then suppose we have a function discretized in a 1D grid and the value at coordinate i is represented by f_i.

There are several ways we can calculate the first derivative

- Forward difference: $f'_i = \frac{f_{i+1} - f_i}{h}$
- Backward difference: $f'_i = \frac{f_i - f_{i-1}}{h}$
- Central difference: $f'_i = \frac{f_{i+1} - f_{i-1}}{2h}$

In this work we mostly use the central difference scheme and from it we can derive formulas to calculate other quantities in 1D like second derivatives, and in higher dimensions we can obtain laplacians, gradients, etc, as shown in Table C.1.

Table C.1: Examples of finite difference formulas in 2D when the grid spacing is $h_x = h_y = 1$.

Quantity	Formula
$\left(\frac{\partial f}{\partial x}\right)_{i,j}$	$\frac{f_{i+1,j} - f_{i-1,j}}{2}$
$\left(\frac{\partial f}{\partial x}\right)_{i,j}$	$\frac{f_{i,j+1} - f_{i,j-1}}{2}$
$\left(\frac{\partial^2 f}{\partial x^2}\right)_{i,j}$	$f_{i+1,j} + f_{i-1,j} - 2f_{i,j}$
$\left(\frac{\partial^2 f}{\partial y^2}\right)_{i,j}$	$f_{i,j+1} + f_{i,j-1} - 2f_{i,j}$
$\left(\frac{\partial^2 f}{\partial x \partial y}\right)_{i,j}$	$\frac{f_{i+1,j+1} + f_{i-1,j-1} - f_{i+1,j-1} - f_{i-1,j+1}}{4}$
$(\nabla^2 f)_{i,j}$	$f_{i+1,j} + f_{i-1,j} + f_{i,j+1} + f_{i,j-1} - 4f_{i,j}$

C.2 FTCS method

The Forward Time Centered Space method is a numerical integration method to solve parabolic partial differential equations, notably the heat/diffusion equation

$$\frac{\partial u}{\partial t} = D\nabla^2 u \tag{C.1}$$

The name of the method comes from the way we discretize the time derivative and the laplacian term. We approximate the time derivative using a forward time scheme

$$\frac{\partial u}{\partial t} \approx \frac{u_{i,j,t+1} - u_{i,j,t}}{\Delta t}$$

and the laplacian (in 2D and when $\Delta x = \Delta y$) by employing centered differences

$$\nabla^2 u \approx \frac{1}{(\Delta x)^2}\left(u_{i+1,j} + u_{i-1,j} + u_{i,j+1} + u_{i,j-1} - 2u_{i,j}\right)$$

Plugging both approximations into the original equation C.1 we get

$$\frac{u_{i,j,t+1} - u_{i,j,t}}{\Delta t} = \frac{1}{(\Delta x)^2}\left(u_{i+1,j} + u_{i-1,j} + u_{i,j+1} + u_{i,j-1} - 2u_{i,j}\right)$$

and finally, rearranging the expression we arrive at

$$u_{i,j,t+1} = u_{i,j,t} + \frac{D\Delta t}{(\Delta x)^2}\left(u_{i+1,j} + u_{i-1,j} + u_{i,j+1} + u_{i,j-1} - 2u_{i,j}\right) \tag{C.2}$$

which tells us the value of the solution to the equation at time $t+1$ only by knowing its value at time t. This very simple idea is based on Euler's method, one of the first algorithms designed for integrating differential equations. It is a very crude method and the accuracy of the final result is dependent on the usage of a small integration step, which is accompanied by a higher computational cost. However, for the equations we need to solve in the model, it is sufficiently accurate for the chosen time step and the integration is fast compared to higher order methods like Runge–Kutta or adaptative algorithms.

However, the stability of the algorithm is dependent on the choice of Δt, Δx and the diffusion coefficient D. In one dimension they must obey the inequality

$$\frac{D\Delta t}{(\Delta x)^2} < \frac{1}{2}$$

In the case of our system, $\Delta x = 1$ so the stability of the integration process is solely dependent on the other two parameters

$$\Delta t < \frac{1}{2D}$$

C.3 Bilinear interpolation

When we have some quantity discretized in a grid, we only know its values in the nodal points belonging to that same grid. However, in some situation we may need to know an approximate value of that quantity somewhere in the middle of the grid, where we do not know it exactly. In order to do so, some kind of interpolation algorithm must be employed in order to find what that value can be, based on the behavior of the neighboring grid points.

Let us suppose we want to know the value of a function ϕ at a point, with coordinates (x, y), that does not belong to the grid. The four closest neighbors that are nodes are located at coordinates $(x_{\text{left}}, y_{\text{down}})$, $(x_{\text{right}}, y_{\text{down}})$, $(x_{\text{right}}, y_{\text{up}})$ and $(x_{\text{left}}, y_{\text{up}})$.

A possible approximation for the value of the function at (x, y) is by averaging the values of the four closest nodes, weighted by the inverse of the distance to those nodes i.e.

$$\phi(x, y) = \sum_i \frac{\phi_i}{(x_i - x)^2 + (y_i - y)^2}$$

where the sum covers the four closest nodes. However, this proved to be an insufficiently good interpolation method and a better one had to be found.

The algorithm that finally guaranteed a good result is called bilinear interpolation and the idea behind is also a weighted average, but this time the weights are the areas of smaller rectangles. These can be constructed using the coordinates of the grid points and of the point where we want to calculate the value of the function as shown in Figure C.1

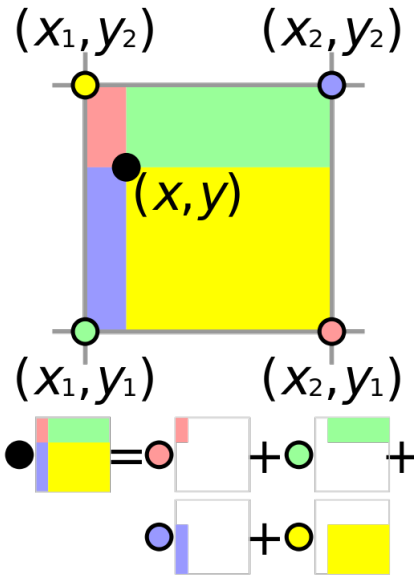

Figure C.1: Bilinear interpolation algorithm [48].

The resulting formula obtained from this method is (using the notation in the figure)

$$\begin{aligned}\phi(x, y) = &\frac{\phi(x_1, y_2)}{(x_2 - x)(y_2 - y)} + \frac{\phi(x_2, y_2)}{(x - x_1)(y - y_1)} \\ &+ \frac{\phi(x_1, y_1)}{(x_2 - x)(y_2 - y)} + \frac{\phi(x_2, y_1)}{(x - x_1)(y_2 - y)}\end{aligned}$$

C.4 Fast Fourier Transform

The first numerical algorithm devised to perform numerical Fourier Transforms was called Discrete Fourier Transform and it consisted on taking a set of data and calculate

$$\tilde{y}(k_n) = \sum_{m=0}^{N-1} y_m e^{-ik_n x_m}$$

where $k_n = n\frac{2\pi}{L}$. This calculation can be written as a

$$\tilde{y}(k_n) = \sum_{m=0}^{N-1} y_m e^{-\frac{2\pi inm}{N}} = \sum_{m=0}^{N-1} y_m (W_{nm})^{nm}$$

with

$$W = e^{-\frac{2\pi i}{N}}$$

which in turn turns into a matrix–vector multiplication.

$$\begin{bmatrix} \tilde{y}_0 \\ \tilde{y}_1 \\ \vdots \\ \tilde{y}_N \end{bmatrix} = \begin{bmatrix} W_N^{0\cdot 0} & W_N^{0\cdot 1} & \dots & W_N^{0\cdot (N-1)} \\ W_N^{1\cdot 0} & W_N^{1\cdot 1} & \dots & W_N^{1\cdot (N-1)} \\ \vdots & \vdots & \ddots & \vdots \\ W_N^{(N-1)\cdot 0} & W_N^{(N-1)\cdot 1} & \dots & W_N^{(N-1)\cdot (N-1)} \end{bmatrix} \begin{bmatrix} y_0 \\ y_1 \\ \vdots \\ y_N \end{bmatrix}$$

As usual with this kind of matricial operation, performing DFT to a set of data with N it scales as $\mathcal{O}(N^2)$. The algorithm is not very efficient and for large datasets the computation can take a very long time.

Around 1960, two IBM researchers, James Cooley and John Tukey devised a new technique that speeds up the computation of numerical Fourier Transforms, reducing the complexity of the algorithm to $\mathcal{O}(N \log N)$. For this reason they called it Fast Fourier Transform, usually referred to by the acronym, FFT. In Table C.2, we can compare the computation time of both algorithms.

Table C.2: Comparison of the two algorithms' performance.

N	DFT	FFT	Speedup
1024	1 s	0.01 s	100×
8192	67 s	0.1 s	670×
65536	71 min	1 s	4260×
1048576	305 hr	20.9 s	53000×

Despite the gigantic difference in efficiency, the FFT algorithm is nothing more than a smarter way to rewrite the expression for the DFT. Let us pick up from the definition of the DFT

$$^{N}\tilde{f}(k) = \sum_{m=0}^{N-1} e^{-\frac{2\pi ikm}{N}} f_m$$

If we split the sum into even and odd terms we get

$$\begin{aligned} ^{N}\tilde{f}(k) &= \sum_{m=0}^{N/2-1} e^{-\frac{2\pi ik(2m)}{N}} f_{2m} + \sum_{m=0}^{N/2-1} e^{-\frac{2\pi ik(2m+1)}{N}} f_{2m+1} \\ &= \sum_{m=0}^{N/2-1} e^{-\frac{2\pi ikm}{N/2}} f_{2m} + W^n \sum_{m=0}^{N/2-1} e^{-\frac{2\pi ikm}{N/2}} f_{2m+1} \end{aligned}$$

If we look at both sums we see that each of them represent another DFT with only half the points i.e.

$$^{N}\tilde{f}(k) =^{N/2} \tilde{f}^{e}(k) + (W^n) \times^{N/2} \tilde{f}^{o}(k)$$

where the upper index "e" or "o" are a tag that tells us if the corresponding points were in the even part of the original sum or in the odd one. This decomposition can be repeated until we are left with only a single value

$$^{N/N}\tilde{f}_k^{eeoeo...oe} = f_m$$

This algorithm is called the *Danielson–Lanczos dizimation* and from the many algorithms that exist to calculate the FFT it is the simplest one.

All that we have to do now is make the correspondence between the sequence of even and odd divisions to the original index of the data. This is performed using an algorithm called binary inversion.

Binary inversion algorithm

1. Invert the sequence of letters, front to back.

$$eeoeo \rightarrow oeoee$$

2. Do the following correspondence

$$e \rightarrow 0$$

$$o \rightarrow 1$$

3. The resulting numeric sequence is the binary representation of m.

$$10100 \rightarrow m = 2^4 + 2^2 = 20$$

Implementing an FFT algorithm is fairly simple, but there are many available libraries that include routines that do the job in a very efficient way, for a single processor but also using distributed computing taking advantage of the many core CPU's. In this work we used the library *FFTW*, considered one of the best scientific software library still in active development [49].

Bibliography

[1] Asfar S Azmi. *Systems biology in cancer research and drug discovery*. Springer, 2012.

[2] Barry M. Prior, H. T. Yang, and Ronald L. Terjung. What makes vessels grow with exercise training? *Journal of Applied Physiology*, 97(3):1119–1128, 2004. ISSN 8750-7587. doi: 10.1152/japplphysiol.00035.2004. URL `http://jap.physiology.org/content/97/3/1119`.

[3] Fabiana Borba Valiatti, Daisy Crispim, Camila Benfica, Bruna Borba Valiatti, Caroline K Kramer, and Luís Henrique Canani. The role of vascular endothelial growth factor in angiogenesis and diabetic retinopathy. *Arquivos Brasileiros de Endocrinologia & Metabologia*, 55(2):106–113, 2011.

[4] Ewa M Paleolog. Angiogenesis in rheumatoid arthritis. *Arthritis Research & Therapy*, 4(3):S81, 2002.

[5] Zoltan Szekanecz, Timea Besenyei, György Paragh, and Alisa E Koch. Angiogenesis in rheumatoid arthritis. *Autoimmunity*, 42(7):563–573, 2009.

[6] J Anthony Ware and Michael Simons. Angiogenesis in ischemic heart disease. *Nature medicine*, 3(2):158–164, 1997.

[7] Peter Carmeliet. Angiogenesis in life, disease and medicine. *Nature*, 438(7070): 932–936, 2005.

[8] N Hudson, M Balsitis, S Everitt, and CJ Hawkey. Angiogenesis in gastric ulcers: impaired in patients taking non-steroidal anti-inflammatory drugs. *Gut*, 37(2):191, 1995.

[9] Sabine A Eming, Bent Brachvogel, Teresa Odorisio, and Manuel Koch. Regulation of angiogenesis: wound healing as a model. *Progress in histochemistry and cytochemistry*, 42(3):115–170, 2007.

[10] Judah Folkman. Tumor angiogenesis: therapeutic implications. *New england journal of medicine*, 285(21):1182–1186, 1971.

[11] Douglas Hanahan and Robert A Weinberg. Hallmarks of cancer: the next generation. *cell*, 144(5):646–674, 2011.

[12] Peter Friedl and Darren Gilmour. Collective cell migration in morphogenesis, regeneration and cancer. *Nature reviews Molecular cell biology*, 10(7):445–457, 2009.

[13] Scuola Superiore Sant'Anna, Pisa, Italy. Human endothelial cells, 2015. URL `http://www.esa.int/spaceinimages/Images/2015/02/Human_endothelial_cells`. [Online; accessed July 29, 2017].

[14] Samarasinghe B. The hallmarks of cancer: Growth factors and cell signaling. *Australian Science*, 2013.

[15] John E Park, Gilbert-A Keller, and Napoleone Ferrara. The vascular endothelial growth factor (vegf) isoforms: differential deposition into the subepithelial extracellular matrix and bioactivity of extracellular matrix-bound vegf. *Molecular biology of the cell*, 4(12):1317–1326, 1993.

[16] Holger Gerhardt, Matthew Golding, Marcus Fruttiger, Christiana Ruhrberg, Andrea Lundkvist, Alexandra Abramsson, Michael Jeltsch, Christopher Mitchell, Kari Alitalo, David Shima, et al. Vegf guides angiogenic sprouting utilizing endothelial tip cell filopodia. *The Journal of cell biology*, 161(6):1163–1177, 2003.

[17] Peter Carmeliet, Valérie Ferreira, Georg Breier, Saskia Pollefeyt, et al. Abnormal blood vessel development and lethality in embryos lacking a single vegf allele. *Nature*, 380(6573):435, 1996.

[18] Napoleone Ferrara, Hans-Peter Gerber, and Jennifer LeCouter. The biology of vegf and its receptors. *Nature medicine*, 9(6):669–676, 2003.

[19] Arndt F Siekmann and Nathan D Lawson. Notch signalling limits angiogenic cell behaviour in developing zebrafish arteries. *Nature*, 445(7129):781–784, 2007.

[20] Mohit Kumar Jolly, Marcelo Boareto, Bin Huang, Dongya Jia, Mingyang Lu, Eshel Ben-Jacob, JoséN Onuchic, and Herbert Levine. Implications of the hybrid epithelial/mesenchymal phenotype in metastasis. *Frontiers in Oncology*, 5:155, 2015. doi: 10.3389/fonc.2015.00155. URL `http://www.ncbi.nlm.nih.gov/pmc/articles/PMC4507461/`.

[21] Lars Jakobsson, Claudio A Franco, Katie Bentley, Russell T Collins, Bas Ponsioen, Irene M Aspalter, Ian Rosewell, Marta Busse, Gavin Thurston, Alexander Medvinsky, et al. Endothelial cells dynamically compete for the tip cell position during angiogenic sprouting. *Nature cell biology*, 12(10):943–953, 2010.

[22] Joseph P Califano and Cynthia A Reinhart-King. The effects of substrate elasticity on endothelial cell network formation and traction force generation. In *Engineering in Medicine and Biology Society, 2009. EMBC 2009. Annual International Conference of the IEEE*, pages 3343–3345. IEEE, 2009.

[23] Cynthia A Reinhart-King, Micah Dembo, and Daniel A Hammer. The dynamics and mechanics of endothelial cell spreading. *Biophysical journal*, 89(1):676–689, 2005.

[24] Sajal Chakraborti, Malay Mandal, Sudip Das, Amritlal Mandal, and Tapati Chakraborti. Regulation of matrix metalloproteinases: an overview. *Molecular and cellular biochemistry*, 253(1-2):269–285, 2003.

[25] José Pinto da Cunha. *Sebenta de Mecânica Clássica II*. 2015.

[26] Lev D Landau and EM Lifshitz. Theory of elasticity, vol. 7. *Course of Theoretical Physics*, 3:109, 1986.

[27] Nikolas Provatas and Ken Elder. *Phase-field methods in materials science and engineering*. John Wiley & Sons, 2011.

[28] Nigel Goldenfeld. *Lectures on phase transitions and the renormalization group*. Addison-Wesley, Advanced Book Program, Reading, 1992.

[29] Lev Davidovich Landau. On the theory of phase transitions. i. *Zh. Eksp. Teor. Fiz.*, 11:19, 1937.

[30] Heike Emmerich. *The diffuse interface approach in materials science: thermodynamic concepts and applications of phase-field models*, volume 73. Springer Science & Business Media, 2003.

[31] Vincent Hakim and Alain Karma. Laws of crack motion and phase-field models of fracture. *Journal of the Mechanics and Physics of Solids*, 57(2):342–368, 2009.

[32] Adam A Wheeler, Bruce T Murray, and Robert J Schaefer. Computation of dendrites using a phase field model. *Physica D: Nonlinear Phenomena*, 66(1-2):243–262, 1993.

[33] Christoph Beckermann, H-J Diepers, Ingo Steinbach, Alain Karma, and Xinglin Tong. Modeling melt convection in phase-field simulations of solidification. *Journal of Computational Physics*, 154(2):468–496, 1999.

[34] Rui DM Travasso, Mario Castro, and Joana CRE Oliveira. The phase-field model in tumor growth. *Philosophical Magazine*, 91(1):183–206, 2011.

[35] Rui DM Travasso, Eugenia Corvera Poiré, Mario Castro, Juan Carlos Rodrguez-Manzaneque, and Aurora Hernández-Machado. Tumor angiogenesis and vascular patterning: a mathematical model. *PloS one*, 6(5):e19989, 2011.

[36] Patrícia Santos-Oliveira, António Correia, Tiago Rodrigues, Teresa M Ribeiro-Rodrigues, Paulo Matafome, Juan Carlos Rodríguez-Manzaneque, Raquel Seiça, Henrique Girão, and Rui DM Travasso. The force at the tip-modelling tension and proliferation in sprouting angiogenesis. *PLoS computational biology*, 11(8):e1004436, 2015.

[37] Makiko Nonomura. Study on multicellular systems using a phase field model. *PloS one*, 7(4):e33501, 2012.

[38] Nabi Nabiollahi, Nele Moelans, Mario Gonzalez, Joke De Messemaeker, Christopher J Wilson, Kristof Croes, Eric Beyne, and Ingrid De Wolf. Microstructure simulation of grain growth in cu through silicon vias using phase-field modeling. *Microelectronics reliability*, 55(5):765–770, 2015.

[39] A.R.A. Anderson; M.A.J. Chaplain. Continuous and discrete mathematical models of tumor-induced angiogenesis. *Bulletin of Mathematical Biology*, 60, 09 1998. doi: 10.1006/bulm.1998.0042.

[40] Alexandre Mezentsev, Roeland MH Merks, Edmond O'Riordan, Jun Chen, Natalia Mendelev, Michael S Goligorsky, and Sergey V Brodsky. Endothelial microparticles affect angiogenesis in vitro: role of oxidative stress. *American Journal of Physiology-Heart and Circulatory Physiology*, 289(3):H1106–H1114, 2005.

[41] Josephine T Daub and Roeland MH Merks. A cell-based model of extracellular-matrix-guided endothelial cell migration during angiogenesis. *Bulletin of mathematical biology*, 75(8):1377–1399, 2013.

[42] Roeland MH Merks, Erica D Perryn, Abbas Shirinifard, and James A Glazier. Contact-inhibited chemotaxis in de novo and sprouting blood-vessel growth. *PLoS computational biology*, 4(9):e1000163, 2008.

[43] Maximilian Heiss, Mats Hellström, Mattias Kalén, Tobias May, Holger Weber, Markus Hecker, Hellmut G Augustin, and Thomas Korff. Endothelial cell spheroids

as a versatile tool to study angiogenesis in vitro. *The FASEB Journal*, 29(7):3076–3084, 2015.

[44] Cristina Borselli, Olimpia Oliviero, Sabrina Battista, Luigi Ambrosio, and Paolo A Netti. Induction of directional sprouting angiogenesis by matrix gradients. *Journal of Biomedical Materials Research Part A*, 80(2):297–305, 2007.

[45] Rui D.M. Travasso, Fernando Sampaio dos Aidos, Pedro Abranches, Anahita Bayani, and Armindo Salvador. P 093 - localized redox relays as a privileged mode of cytoplasmic hydrogen peroxide signaling. *Free Radical Biology and Medicine*, 108, Supplement 1:S49 –, 2017. ISSN 0891-5849. doi: https://doi.org/10.1016/j.freeradbiomed.2017.04.178. URL `http://www.sciencedirect.com/science/article/pii/S0891584917303817`. Abstracts of the {OCC} World Congress and Annual SFRR-E Conference 2017 Metabolic Stress and Redox Regulation Berlin, Germany 21-23 June 2017.

[46] Maurício Moreira Soares. Coupling blood flow and growing vasculature in three dimensions, 2015.

[47] Hugo Rafael Lopes Ferreira. Model for angiogenesis in three dimensions taking into account tissue elasticity, 2016.

[48] Cmglee. URL `https://en.wikipedia.org/wiki/Bilinear_interpolation`. [Online; accessed July 29, 2017].

[49] Matteo Frigo and Steven G Johnson. The design and implementation of fftw3. *Proceedings of the IEEE*, 93(2):216–231, 2005.